Chapter GR (Gravity Modeling)

GRAVITY DATA PROCESSING, MODELING, AND INTERPRETATION IN SUPPORT OF STRUCTURAL STUDIES IN THE NORTHERN PART OF THE ARCTIC NATIONAL WILDLIFE REFUGE, ALASKA

by Richard W. Saltus[1], Robert L. Morin[2], Jeffrey D. Phillips[1], and Michael W. Webring[1]

in The Oil and Gas Resource Potential of the 1002 Area, Arctic National Wildlife Refuge, Alaska, by ANWR Assessment Team, U.S. Geological Survey Open-File Report 98-34.

1999

[1] U.S. Geological Survey, MS 964, Denver, CO 80225
[2] U.S. Geological Survey, MS 989, Menlo Park, CA 94025

TABLE OF CONTENTS

Abstract

In this report we describe our gravity interpretation of an onshore/offshore region centered on the coastal plain of the Arctic National Wildlife Refuge (ANWR) in northeastern-most Alaska. The main conclusions from our interpretation are: (1) low gravity values over much of the ANWR coastal plain reflect the thickness of the sedimentary section that overlies the pre-Mississippian basement rocks; (2) a high gravity ridge in the eastern part of the study area (in the Niguanak region) is caused by a high-density body in the mid to lower crust, possibly a failed rift arm containing mafic rocks; (3) a small, but significant, density contrast (0.05 g/cm^3) between deformed and undeformed sediments is required to fit the gravity gradients on the southern margin of the coastal plain; (4) the gravity gradient on the southern margin of the coastal plane can be modeled using a relatively high density (2.85 g/cm^3) for thrusted basement rocks to the south; (5) a residual gravity map produced by wavelength filtering delineates structures in the upper 3 km (within the post-Cretaceous sedimentary section); (6) areas and volumes of these structures can be estimated based on a three-dimensional model - these values are upper limits on sizes of possible structural hydrocarbon traps in that region; (7) subtle gravity highs in the northwest portion of the coastal plain may correlate spatially with turbidite mounds identified by seismic stratigraphy.

Introduction

The gravity interpretations discussed in this report are focused on understanding subsurface geologic structure in the coastal plain of the Arctic National Wildlife Refuge (ANWR) in northeastern Alaska (Fig. GR1). A region comprising much of the coastal plain has been designated the 1002 area in reference to legislation passed by the U.S. Congress in 1981 that permitted preliminary oil and gas exploration activities in the area (Bird and Magoon, 1987). In order to understand the regional context of gravity features within the 1002 area, our maps and interpretations extend to the south into the Brooks Range and to the north offshore.

The 1002 area consists of a sedimentary basin containing undeformed to highly deformed sequences of clastic rocks (Grow and others, Chap. NA). Exposures of the rocks are rare within the basin, due to the pervasive tundra cover and Pleistocene to Holocene surficial deposits (Bader and Bird, 1986). The Cretaceous to Pliocene sandstones and shales within the upper part of the basin were derived from the Brooks Range to the south, and are called the Brookian stratigraphic sequence. The Mississippian to Cretaceous shale,

sandstone, and carbonate rocks within the lower part of the basin were derived from the north, and are called the Ellesmerian stratigraphic sequence. The underlying pre-Mississippian basement rocks at depths of 3 to 6 kilometers include argillite, phyllite, quartzite, volcanic rocks, carbonate rocks, and granite (Bird and Molenaar, 1987).

The earliest published gravity measurements for northeastern Alaska (Thiel and others, 1958) consist of a half-dozen measurements along the Beaufort Sea coast and on the upper reaches of several rivers to the south of the Brooks Range. Subsequent data collection by the U.S. Geological Survey (USGS) were included in the first regional gravity maps of the area (Barnes and others, 1976). Kososki and others (1978) published the first regional interpretation of gravity data for the region; they concluded that "major post-Carboniferous sedimentary basins whose centers lie offshore on the Beaufort Shelf extend onshore" in the 1002 area. They were hampered in their efforts to perform detailed interpretation by the lack of additional information (such as seismic data) and by the difficulty of calculating regional gravity corrections (such as terrain corrections, offshore Bouguer corrections, and isostatic corrections as discussed below). Robbins (1987) used an extensive proprietary gravity data set (the same data used in this report) to construct detailed two-dimensional gravity models of Bouguer gravity anomalies along six north-south seismic lines. He concluded that the gravity anomalies within the 1002 area were dominantly controlled by the depth to the pre-Mississippian basement in the region. In addition, he speculated that the offshore Dinkum graben extends onshore to the south of Barter Island and may have once extended to the east to join with the free-air gravity low off of Demarcation Bay.

This report documents data processing and modeling done in conjunction with seismic and structural studies (Grow and others, Chap. NA). Gravity data processing is an important first step in the interpretation, so it receives detailed discussion. The next topic is discussion of a set of intersecting two-dimensional gravity models centered along seismic lines in the 1002 area; these models define large-scale structural elements within the sedimentary section and the basement. Next, filtering techniques and three-dimensional analysis are used to model structures within the Brookian section. Finally, estimates of area and volume of the larger of these structures are made to assist in evaluation of possible oil and gas trap sizes.

Gravity Data Processing

The gravity data processing builds on the complete Bouguer anomaly data set published on a 2-mGal contour map at a scale of 1:500,000 by Robbins (1987). As documented by Robbins (1987), this data set includes proprietary data collected by Photo-gravity (regional grid) and by Geophysical Service Inc. (closely-spaced coverage along seismic lines) as well as irregularly spaced public-domain data collected by the USGS (Kososki and others, 1978; T.R. Bruns and M.A. Fisher, unpub. data, 1984). In addition, data are included from the Okpilak batholith region to the south of the 1002 area collected by Petersen (1995) and offshore ship-track data obtained from the National Geophysical Data Center (NGDC) in Boulder, Colo.

The goal of the gravity processing is twofold: (1) to enhance the ability to recognize and model structural features of the Brookian sedimentary section within the 1002 area, and (2) to give an understanding of large-scale density features of the pre-Mississippian basement. To achieve these goals, we must remove the large regional gravitational effects caused by the contrast in crustal density structure between the topographically high continental crust of the Brooks Range to the south and the deep offshore Canada basin to the north. This is accomplished by processing the gravity data to produce isostatic residual gravity anomalies (Simpson and others, 1986).

Traditional gravity data processing consists of a series of steps, each designed to remove a gravitational effect that can be calculated with well-constrained assumptions. The gravity method has a rich history which is reflected in the terminology applied to the gravity values obtained at each step. Unfortunately, this historical terminology and the use of gravity values from the various steps of the reduction process in interpretive reports can hinder understanding and comparison of gravity models and results.

The actual measured gravity value is termed “observed gravity”; it is a number which ranges from about 9.78 to 9.83 m/s^2 over the Earth. The primary reason for variation in observed gravity is the shape and rotational velocity of the Earth which can be calculated as a function of latitude. A secondary cause for variation in gravity is elevation (distance from the center of mass of the Earth). These latitude and elevation effects are calculated and removed from observed gravity to obtain “free-air gravity.” Free-air gravity varies by several hundred milligals (1 mGal = 10^{-5} m/s^2) over the Earth. Free-air gravity values are dominated by a short-wavelength correlation with topography on land and by long-wavelength anomalies at

major crustal boundaries (such as the continent to ocean transition; Fig. GR2).

The next step in traditional gravity data reduction is to calculate and remove the effects of topographic masses (above sea level) from the free-air gravity to obtain "Bouguer gravity" (Fig. GR2). Most gravity studies employ Bouguer gravity for modeling on land; many studies employ free-air gravity for modeling offshore. Studies that span onshore and offshore areas often employ hybrid maps with Bouguer gravity on land and free-air gravity offshore (for example, Robbins, 1987). Bouguer and free-air gravity values agree at sealevel allowing the construction of seamless onshore-offshore maps, but care must be taken in interpreting and especially in modeling these hybrid maps because of the differing assumptions on- and offshore. To apply a Bouguer correction to offshore data, the effect of the water-filled ocean is calculated and removed from the free-air data. To avoid the problems of working with a hybrid map, we have applied this correction to ship-track gravity data obtained from NGDC.

Long-wavelength trends in Bouguer gravity mirror topography; Bouguer gravity is generally low over high mountains and high over the ocean basins. The topographic correlation led to the theory of isostasy which states that lithospheric buoyancy plays a major role in supporting topography and bathymetry; high mountains are supported by low-density "roots" at depth, deep basins are underlain by relatively high-density material.

The 1002 area lies in a region of large regional gradient in Bouguer gravity caused by the effects of the deep isostatic masses that support the extreme differences in topography between the Brooks Range to the south and the Arctic ocean basin to the north. In order to understand and model features within and surrounding the 1002 area we must understand and remove this regional gradient. There are numerous ways to approach the problem of regional gradient removal, all require some assumptions about the deep structure of the crust and upper mantle. In the absence of additional information on deep structure, we have chosen to use a simple model of isostatic balance - an Airy isostatic model (Simpson and others, 1986); the Airy isostatic model is relatively insensitive to the exact choice of the model parameters (Simpson and others, 1986). The parameters of our isostatic model are:

1. Depth to isostatic root ("Moho") at sea level = 25 km
2. Average density of topographic masses = 2.67 g/cm^3
3. Density contrast at the isostatic root ("Moho") = 0.4 g/cm^3

In a study of gravity data in the National Petroleum Reserve, Alaska (NPRA; located to the west of ANWR), McEntee (1987) found that application of an Airy isostatic regional aided in the analysis of structure within the Ellesmerian and Brookian sedimentary sections. For that study the following isostatic parameters were used: (1) depth to isostatic root ("Moho") at sealevel = 34 km, (2) average density of topographic masses = 2.58 g/cm^3, (3) density contrast at the isostatic root ("Moho") = 0.35 g/cm^3. Although it has little effect on the form of the isostatic regional, our parameters, listed above, are in better agreement with the seismic interpretations of Fuis and others (1995) than the parameters used previously by McEntee (1987).

The differences between the gravity values obtained at the various stages of the reduction process are illustrated in a south to north regional profile (Fig. GR2). Note that a hybrid Bouguer/free air profile would be impossible to fit with a single integrated model. The isostatic residual gravity values (red line, Fig. GR2), reflect lateral density contrasts within the mid to upper crust; they form the starting point our gravity modeling.

In map view, the isostatic residual gravity field of the region surrounding the 1002 area (Fig. GR3; Pl. GR1) shows a prominent gravity low associated with sediments of the 1002 area. This low is flanked to the south by high gravity values in the Brooks Range (with the exception of a gravity low that occurs over exposures of the Okpilak batholith; Petersen, 1995) and to the north by a large off-shore gravity high associated with high density material within the basement of the continent-to-ocean transition zone. Detailed interpretation of these data are given in several sections below.

Rock Density Information

Gravity anomalies are caused by lateral variations in the density of Earth materials; to construct gravity models such as those in the following section, we must make assumptions about these density contrasts for the rock units we are modeling (alternately, we could assume the shape of the rock units and solve for the densities). Ideally, this is guided by actual bulk density measurements of these units in situ (best accomplished by a series of borehole gravity surveys distributed throughout the region). However, optimum density information is rarely, if ever, available, and model densities are usually based on some surface samples and on expectations based on measurements made elsewhere on similar rock lithologies.

Density measurements on surface rock samples in the region surrounding the 1002 area have been published by Kososki and others (1978; 167 samples) and by Petersen (1995; 11 samples). Robbins (1987) reported density estimates from gamma-gamma density well logs, primarily along the Canning River on the western boundary of the 1002 area (Fig. GR1).

These published densities, as well as density estimates by Nelson (Chap. PP) and by us from scaled multi-trace borehole data plots, are plotted on Figure GR4. Rock density generally increases with age of the rocks and ranges from less than 2.0 (Sagavanirktok Formation) to greater than 3.0 g/cm^3 (basement meta-volcanics) in rocks from this region. Many of the densities measured on pre-Mississippian basement rock types exceed 2.7 g/cm^3. Densities measured on pre-Mississippian volcanic and volcaniclastic rocks average greater than 2.8 g/cm^3; a density of 3.2 g/cm^3 is reported from a metabasalt (Kososki and others, 1978; sample 140) collected on the north flank of the Sadlerochit Mountains on the footwall block of the frontal thrust.

Two-dimensional Gravity Models

We have made two- and two-and-one-half-dimensional gravity models using eight density categories (Fig. GR5) along three south-north profiles located along seismic traverses and on a fourth east-west profile that intersects the other three. Here is a list of the four profiles with a brief discussion of details specific to each profile:

1. 84-6 & 85-5 (Figs. GR6 and GR7; S-N profile in western part of the 1002 area). Two alternate interpretations are given for this profile. The first (Fig. GR6) is based on modeling constrained by the seismic interpretations (Grow and others, Chap. NA). The second (Fig. GR7) is based on seismic interpretation and balanced cross section modeling of Cole (Chap. SM). In detail, the combined over and underthrust geometry of the deformed sedimentary rocks into the undeformed sedimentary rocks (Fig. GR6; Grow and others, Chap. NA) fits the gravity data better than the underthrust-only interpretation (Fig. GR7; Cole, Chap. SM). To the south of the seismic line (into the Sadlerochit and Shublik Mountains), the details of the balanced cross section (Fig. GR7; Cole, Chap. SM) make the gravity modeling more realistic there than on the geologically unconstrained original model (Fig. GR6).

2. 84-14 (Fig. GR8; S-N profile in the center of the 1002 area, crosses the Marsh Creek anticline). The high density "thrust sheet" body at the southern end of the profile is ad hoc. Some kind of higher density body is required,

but the details of the geometry are not well constrained off the end of the seismic line. The modeled body represents a simple body that mimics thrust geometries in Cole's (Chap. SM) balanced cross section to the west. As shown on this profile, and discussed below in the section on three-dimensional gravity models, the Marsh Creek anticline is asymmetric in cross-section. For a more detailed account of this structure, see the aeromagnetic interpretation of Phillips (Chap. AM). A distinct residual gravity high of about 3 mGal coincides with the crest of the Marsh Creek anticline (Robbins, 1987). We make an estimate of the volume of the Marsh Creek structure (Table GR1) as discussed in a later section of the report.

3. 85-50 (Fig. GR9; S-N profile in eastern part of the 1002 area, crosses the Niguanak high). This profile is of particular interest to the oil and gas assessment effort because it crosses the Niguanak structure (Grow, Chap. NA). The gravity model indicates that rocks with pre-Mississippian basement densities occur within the deeper parts of the Niguanak structure. To the north of the Niguanak structure we have modeled a high density (+0.2 g/cm^3 density contrast, 2.9 g/cm^3 absolute density) body that joins to the higher density offshore body present in all the south-to-north profiles. This body is placed at the shallowest level permitted by the seismic interpretation, but it may lie deeper in the crust. Our working hypothesis is that this body represents mafic rocks contained in a failed rift (aulocogen) that formed during rifting of the Arctic Alaska composite terrane from Canada at the onset of Canada basin formation about 160 Ma (Plafker and Berg, 1994). The body is modeled in two-and-one-half dimensions; see Figures GR10 and GR11 for several views of this body.

4. E-W (Fig. GR10; West to east profile in northern part of the 1002 area, intersects with the S-N profiles). This profile ties together the previously discussed south-to-north profiles (Fig. GR11 shows how they fit together). The high-density body in the lower crust on the eastern end of the line is described above in the discussion on profile 85-50.

The south-to-north models extend beyond the edges of the seismic lines to include important gravity anomalies to the south over the Brooks Range and to the north across the passive rift margin at the continental slope. The brightest reflectors recognized on the depth-migrated seismic lines are displayed (Grow and others, Chap. NA) and used as structural guides for modeling. The models are simplified to use a minimum number of density layers (listed on Fig. GR5). Density contrasts are consistent with the density data discussed above (summarized on Fig. GR4). Density contrasts are relative to an assumed pre-Mississippian basement density of 2.7 g/cm^3 (Fig. GR4). The

lithologic interpretations of the density bodies are based on the density/stratigraphic relations summarized in Fig. GR4 and on structural interpretation of the seismic data (Grow and others, Chap. NA).

Common elements of the S-N profiles (Fig. GR5; also see Fig. GR11 for a perspective overview of all the profiles) include:

1. A high density (contrast of +0.15 g/cm^3, yielding a absolute density of 2.85 g/cm^3) body that represents basement thrust sheets in the Sadlerochit and Shublik Mountains and may deepen to the east. Note that the density of this body is lower (2.8 g/cm^3) in the alternate model of seismic line 84-6/85-8 (Fig. GR7). The relatively high absolute densities implied for these thrusted bodies is problematic and might imply that a smaller value for average basement density is more appropriate (for example 2.65 g/cm^3 instead of 2.7 g/cm^3);
2. A low density (contrast of -0.15 g/cm^3, absolute density of 2.55 g/cm^3) body along the southern margin of the 1002 area that may represent deformed sedimentary rocks (the systematically higher densities verses the relatively undeformed sedimentary rocks to the north may be the result of more compaction and de-watering of these rocks);
3. Lower density (mostly density contrast of -0.2 g/cm^3 with lower density surficial layers toward the west, absolute densities range from 2.5 to 2.35 g/cm^3) bodies representing relatively undeformed sedimentary rocks;
4. A very high density (contrast of +0.3, absolute density 3.0) body in the mid to lower crust offshore that may reflect mafic intrusions related to continental breakup;
5. A high density (contrast of +0.2, absolute density of 2.9) mid to lower crustal body beneath the central portion of 85-50 (in the Niguanak region) that we suggest may be mafic rocks in a failed rift arm (aulacogen) related to the opening of the Canada basin and the rotation of Arctic Composite Terrane beginning at about 160 Ma (Plafker and Berg, 1994). Under this interpretation, this north-south oriented gravity ridge represents an extension of the east-west trending continental edge anomaly (discussed in 4, above).

Wavelength Filtering and Three-dimensional Gravity Models

In order to separate the fine scale (shorter wavelength) gravity effects of shallow structures within the Brookian section (such as the Marsh Creek anticline shown in Fig. GR8) from the broader scale (longer wavelength) effects arising from the depth to and composition of pre-Mississippian basement, we have used the Fourier transform to analyze the spectrum of the isostatic residual gravity (Fig. GR12). Based on this modeling we have defined a set of three wavelength filters to separate the gravity field by

average depth of sources (Fig. GR12). The filters tend to emphasize source depths as follows:

(1) Long wavelengths: mostly deeper than 3 km.
(2) Intermediate wavelengths: from about 300 m to 3 km.
(3) Short wavelengths: shallower than about 300 m.

We have produced two maps: (1) a regional map that shows the long wavelengths (Fig. GR13) and (2) a residual map that combines the intermediate and short wavelengths (Fig. GR14 and GR2). The residual map is restricted to the 1002 area because that is the only part of the study area with sufficient data coverage to justify detailed interpretation of the fine-scale features. The broad features shown in the long-wavelength (low-pass) regional map have been modeled in our two-dimensional models discussed above. We will now concentrate on three-dimensional modeling of the features in the intermediate and short wavelength (high-pass) residual map.

To illustrate the nature of the structures reflected in the high-pass residual map we have constructed several detailed two-dimensional models that incorporate constraints from seismic interpretations (Grow and others, Chap. NA) and from modeling of aeromagnetic data (Phillips, Chap. AM). These models (Figs. GR15, GR16, and GR17) show simple density bodies that fit the residual data. These bodies are simplified and the details of their geometries are not well constrained, but they show that bodies with thicknesses of several kilometers and density contrasts ranging from 0.05 to 0.10 g/cm^3 are consistent with structural patterns from the seismic and aeromagnetic interpretations.

To assist in estimating sizes of potential oil and gas trapping structures, we calculated the areas and volumes of shallow sources that fit the high-pass residual gravity based on a three-dimensional density model (Fig. GR18). This density model is a surface with a density contrast of 0.1 g/cm^3 (as would be formed by undulations in the contact between the lower density Sagavanirktok Formation and underlying higher density Canning Formation within the upper part of the Brookian section; Fig. GR4). To produce this surface, we (1) added 5 mGal to the residual gravity values to produce a map with all positive values, (2) made an initial estimate of the depth to the surface using the one-dimensional gravity slab formula ($t = g/2\pi G\rho$; t = thickness in km, g = residual gravity value, $2\pi G \approx 42$ mGal/km g/cm^3, ρ = density contrast of 0.1 g/cm^3), (3) performed a three-dimensional forward calculation of the gravity field produced by this surface (using a program by Rick Blakely, USGS, Menlo Park), (4) subtracted this calculated field from

the high-pass residual gravity map (Fig. GR14 and GR2), and (5) adjusted the depth to the surface as dictated by the difference. We repeated steps 4 and 5 twice to achieve a good match between the calculated field and the high-pass residual gravity map.

Rather than incorporate enough constraints to accurately model the exact form of density interface that causes these short-wavelength patterns, we use this simple model to determine the amount of anomalous mass (i.e., the volume of the structures times the density contrast), a quantity that is uniquely determined by the gravity values (this follows from Gauss' law; Blakely, 1995, p. 59). We use the anomalous mass estimate to construct robust estimates of structural areas and volumes from the three-dimensional density model. From this analysis we identified 12 distinct structures (Fig. GR19). Most of these structures form gravity highs, implying that high density rocks form the cores of the structures. Two of the anomalies (numbers 7 and 8) form gravity lows (these represent the Aichilik high; Grow, and others Chap. NA) indicating that the core of the structure has relatively lower density compared to adjacent rocks. The areas of these structures range from 45 to 350 km^2 and the volumes range from 7 to 70 km^3 (Table GR1). These values, along with constraints from seismic interpretation (Grow and others, Chap. NA), contributed to structural trap parameters for thin-skinned thrust-belt (Bird, Chap. AO; Perry and others, Chap. P8).

In this analysis we have not attempted to model the sources of some subtle wavelength residual gravity anomalies that lie to the northwest of the Marsh Creek anticline in the undeformed part of the 1002 area. These subtle anomalies may be related to turbidite mound features as identified by Houseknecht and Schenk (Chap. P2) from detailed seismic stratigraphy. These subtle gravity highs may reflect stratigraphic regions containing density inversions (higher density sediments above lower density sediments) as has been postulated (Vogt, 1997) as a condition for initiating buoyancy instabilities that give rise to mound fields in the Norway Basin.

Conclusions

1. Isostatic residual gravity anomalies contain long-wavelength features that are primarily sensitive to the depth of the pre-Mississippian basement over most of the 1002 area.
2. An exception to this depth-to-basement correlation occurs in the Niguanak high region in the eastern part of the 1002 area. As modeled along seismic line 85-50 and on the E-W transverse gravity profile, the gravity ridge in this region is caused by a high-density body (mafic rocks in a failed

rift arm that originated during the formation of the Canada basin?) in the mid to lower crust rather than an extreme shallowing of pre-Mississippian basement. Note, however, that the Niguanak structure itself (Fig. GR9) is made up of rocks with pre-Mississippian basement density (2.7 g/cm^3); the inferred mafic rocks are based on our gravity modeling and lie at greater depths (however, depth to the top of these rocks is not well constrained by our analysis).

3. A systematic contrast (0.05 g/cm^3) between deformed and undeformed sediments is required to fit the gravity gradient along the southern margin of the 1002 area. This density contrast may indicate a greater degree of compression and de-watering of the deformed sediments relative to the undeformed sediments; this contrast could be an important indication of a difference in physical properties of interest in petroleum reservoir characterization (Nelson, Chap. PP).

4. A high-density (modeled at 2.85 g/cm^3) body ("thrust sheet") is used to the south of the 1002 area to match the gravity high along that flank.

5. Short-wavelength isostatic residual gravity features arise primarily from structures in the upper 3 km (within the Brookian sedimentary section). A prominent gravity high ridge follows the Marsh Creek anticline. Most other structural anticlines are reflected as gravity highs. However, at least one anticline, the Aichilik high along the southeast portion of 1002, is coincident with a gravity low. We have calculated areas and volumes of these structures based on a three-dimensional gravity model; these values are upper limits on sizes of structural traps for the thin-skinned thrust-belt play (Bird, Chap. AO; Perry, Chap. P8).

6. Subtle, roughly equi-dimensional anomalies (highs) in the northwest portion of the 1002 area (undisturbed area), may correlate spatially with turbidite mounds in the turbidite play (Bird, Chap. AO) identified by seismic stratigraphy analysis (Houseknecht and Schenk, Chap. P2).

Acknowledgments

We have benefited from extensive interaction with other USGS ANWR project personnel including Ken Bird, John Grow, Chris Potter, Bill Perry, John Kelley, Fran Cole, Tom Moore, Phil Nelson, and others. We thank Steve Robbins for providing data and notes from his previous work in the area. Dave Ponce and Tien Grauch provided helpful reviews of this report.

References

Bader, J.W., and Bird, K.J., 1986, Geologic map of the Demarcation Point, Mt Michelson, Flaxman Island, and Barter Island quadrangles,

northeastern Alaska: U.S. Geological Survey Miscellaneous Geologic Investigations Map I-1791, scale 1:250,000.

Barnes, D.F., Kososki, B.A., Mayfield, C.F., Robbins, S.L., and Trailleur, I.L., 1976, Gravity data from Mt. Michelson, Flaxman Island, Demarcation Point, and Barter Island quadrangles, Alaska: U.S. Geological Survey Open-File Report 76-258, 4 sheets, scale 1:250,000.

Beyer, L.A., and Clutsom, F.G., 1989, Basic data and preliminary density and porosity profiles from three borehole gravity surveys made in the Kuparuk River and Prudhoe Bay Oil fields, Alaska: U.S. Geological Survey Open-File Report 89-369, 26p.

Blakely, R.J., 1995, Potential Theory in Gravity & Magnetic Applications: Cambridge University Press, New York, 441 p.

Bird, K.J. and Magoon L., eds., 1987, Petroleum Geology of the Northern Part of the Arctic National Wildlife Refuge, Northeastern Alaska: U.S. Geological Survey Bulletin 1778, 329 p.

Bird, K.J., and Molenaar, C.M., 1987, Stratigraphy, *in* Bird, K., and Magoon, L., eds, Petroleum Geology of the Northern Part of the Arctic National Wildlife Refuge, Northeastern Alaska: U.S. Geological Survey Bulletin 1778, p. 37-59.

Fuis, G.S., Levander, A.R., Lutter, W.J., Wissinger, E.S., Moore, T.E., Christensen, N.I., 1995, Seismic images of the Brooks Range, Arctic Alaska, reveal crustal-scale duplexing: Geology, v. 23, n. 1, p. 65-68.

Kososki, B.A., Reiser, H.N., Cavit, C.D., and Detterman, R.L., 1978, A gravity study of the Northern Part of the Arctic National Wildlife Range, Alaska: U.S. Geological Survey Bulletin 1440, 21p.

McEntee, R.A., 1987, The accurate modeling and removal of regional sources of the gravitational field, M.S. Thesis, Colorado School of Mines, Golden, CO., 184 p.

Petersen, C.A., 1995, Gravity Modeling of the Okpilak Batholith, Northeastern Brooks Range, Alaska: Master of Science Thesis, University of Alaska Fairbanks, unnumbered, about 100 p.

Plafker, G., and Berg, H.C., 1994, Overview of the geology and tectonic evolution of Alaska: in Plafker, G., and Berg, H.C., eds, The Geology

of Alaska: Boulder, Colorado, Geological Society of America, The Geology of North America, v. G-1, p. 989-1021.

Robbins, 1987, Gravity interpretation of the coastal plain: in Bird, K.J, and Magoon, L.B., eds., Petroleum Geology of the Northern Part of the Arctic National Wildlife Refuge, Northeastern Alaska: U.S. Geological Survey Bulletin 1778, p. 219-224.

Simpson, R.W., Jachens, R.C., Blakely, R.J., and Saltus, R.W., 1986, A new isostatic residual gravity map of the conterminous United States with a discussion on the significance of isostatic residual anomalies: Journal of Geological Research, v. 91, n. B8, p. 8348-8372.

Thiel, E., Ostenso, N.A., Bonini, W.E., and Woollard, G.P., 1958, Gravity measurements in Alaska: Woods Hole Oceanographic Institute Technical Report Reference 58-54, 104 p.

Vogt, P.R., 1997, Hummock fields in the Norway Basin and eastern Iceland Plateau: Rayleigh-Taylor instabilities? Geology, v. 25, no. 6, p. 531-534.

Click here or on this symbol in the toolbar to return.

TABLE GR1

Area and volume statistics for 12 gravity-defined structures in the Thin-skinned Thrust-belt Play, 1002 area, ANWR, Northern Alaska

Str #	Floor(km)	Floor(kft)	Area(km^2)	Area(k acres)	Vol(km^3)	Vol(acre-ft)	StrHt(km)	StrHt(kft)	
1	-1.8	-5.9	185	45.7	68.9	5.58E+07	0.373	1.223	MCA* - eastern part
2	-1.8	-5.9	212	52.4	47.1	3.81E+07	0.222	0.729	MCA* - western part
3	-1.8	-5.9	68	16.8	13.9	1.12E+07	0.204	0.669	
4	-1.8	-5.9	104	25.7	30.2	2.45E+07	0.290	0.952	Shallow Niguanik structure
5	-1.8	-5.9	74	18.3	7.2	5.86E+06	0.098	0.321	
6	-1.8	-5.9	81	20.0	8.0	6.49E+06	0.099	0.324	
7	-1.8	-5.9	97	24.0	27.0	2.19E+07	0.279	0.915	Aichilik High - eastern part
8	-1.8	-5.9	114	28.2	45.5	3.69E+07	0.399	1.310	Aichilik High - western part
9	-1.8	-5.9	71	17.5	11.1	8.98E+06	0.156	0.512	
10	-1.8	-5.9	45	11.1	7.2	5.85E+06	0.161	0.527	
11	-1.8	-5.9	349	86.2	71.1	5.76E+07	0.204	0.668	
12	-1.8	-5.9	157	38.8	20.2	1.64E+07	0.129	0.423	
		totals	1557	384.6	357.5	2.90E+08			
		average	130	32.0	29.8	2.41E+07	0.218	0.714	
		std dev	86	21.1	23.3	1.89E+07	0.100	0.328	

Column definitions:

Str # = Structure number (see Fig. GR19)
Floor = depth to the bottom of the structure, measured from surface
Area = area of structure at floor depth
Vol = volume of structure above floor depth
StrHt = volume of structure divided by area (gives average height of structure)

Notes:

1. Structures defined by 3D iterative modeling of high-pass residual gravity using a density contrast of 0.1 gm/cm^3.
2. Residual gravity filters defined by matched filtering (see Fig. GR12).
3. Most features modeled as positive density contrast (anticlines with denser core), except for structures #7 and #8.
4. Structures #7 and #8 modeled with negative density contrast (lower density core).
5. All areas and volumes calculated on a 1 x 1 km grid.
6. MCA* = Marsh Creek Anticline

Figure GR1. Location map

Location map for the study area showing: (1) topography, shoreline, and bathymetry, and selected structural features (2) the 1002 area boundary, (3) locations of gravity profiles and seismic lines discussed in this report, and (4) well locations for wells cited in this report. MCA = Marsh Creek anticline; NH = Niguanak high; AH = Aichilik high.

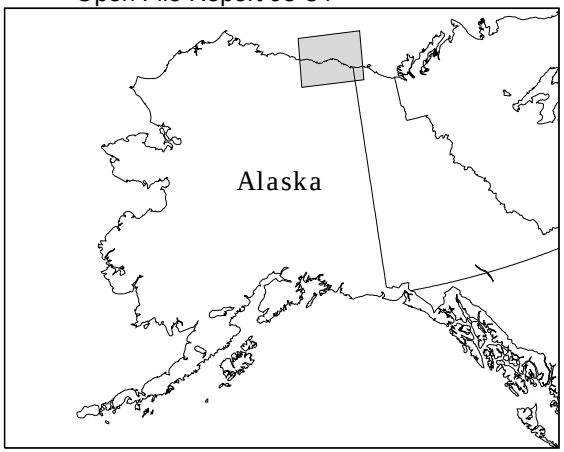

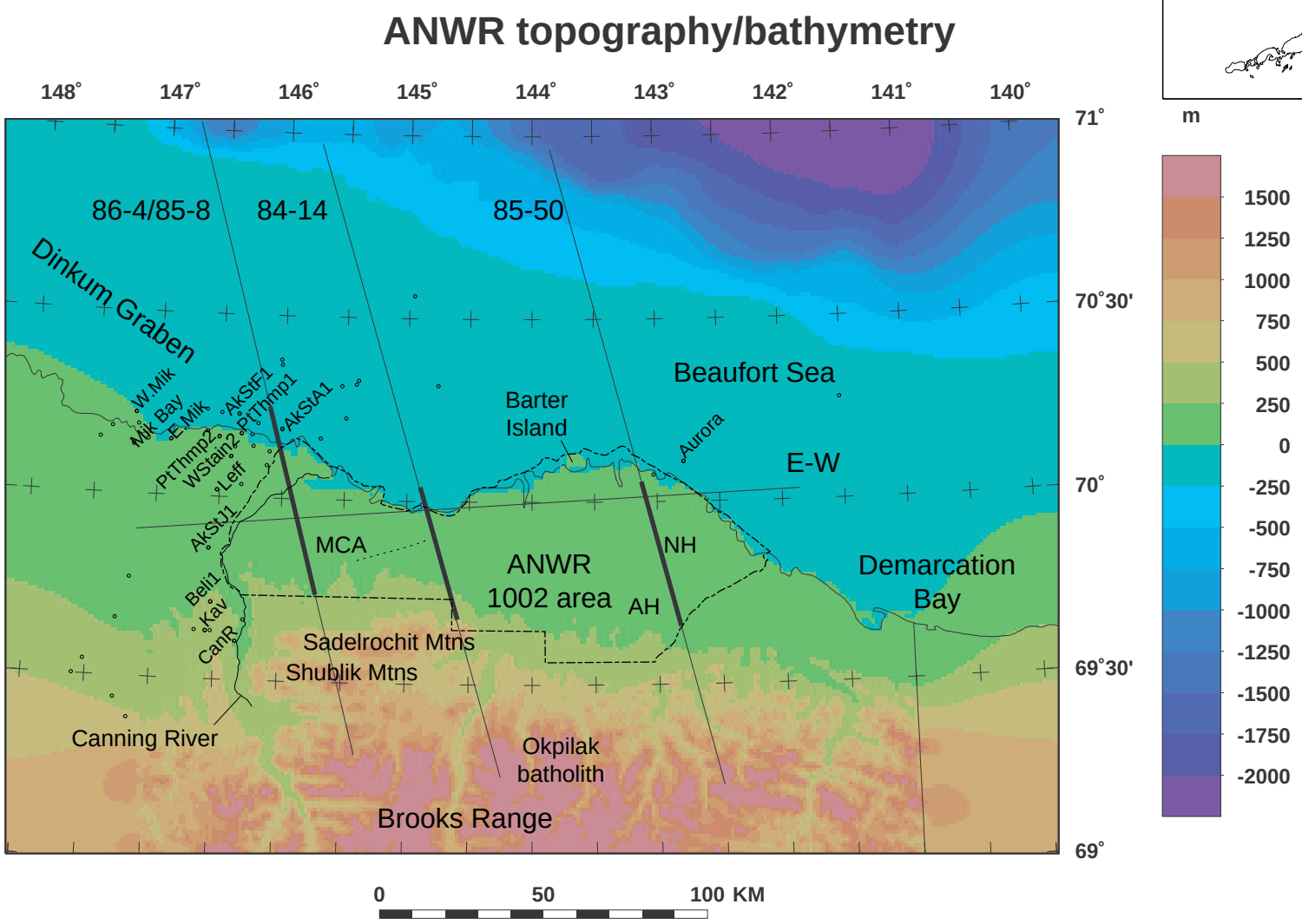

Figure GR1 - Saltus and others, 1998

Figure GR2. Gravity corrections - south to north profile

Illustration of the definition of three commonly used gravity anomaly values: (1) free-air gravity, (2) Bouguer gravity, and (3) isostatic residual gravity. Free-air gravity (green profile) is a sum of the gravitational effects of all bodies shown in the model. Bouguer gravity (black profile) is free-air gravity with the effects of topography and bathymetry removed. Isostatic residual gravity (red profile) is Bouguer gravity with the effects of deep isostatic roots (and anti-roots) removed. Isostatic residual gravity is used as the basis for modeling throughout this report. The calculations for this illustration were done in two dimensions (i.e., the bodies shown extend to infinity in and out of the plane of the figure), so the gravity values do not agree exactly with measured values arising from the three-dimensional Earth.

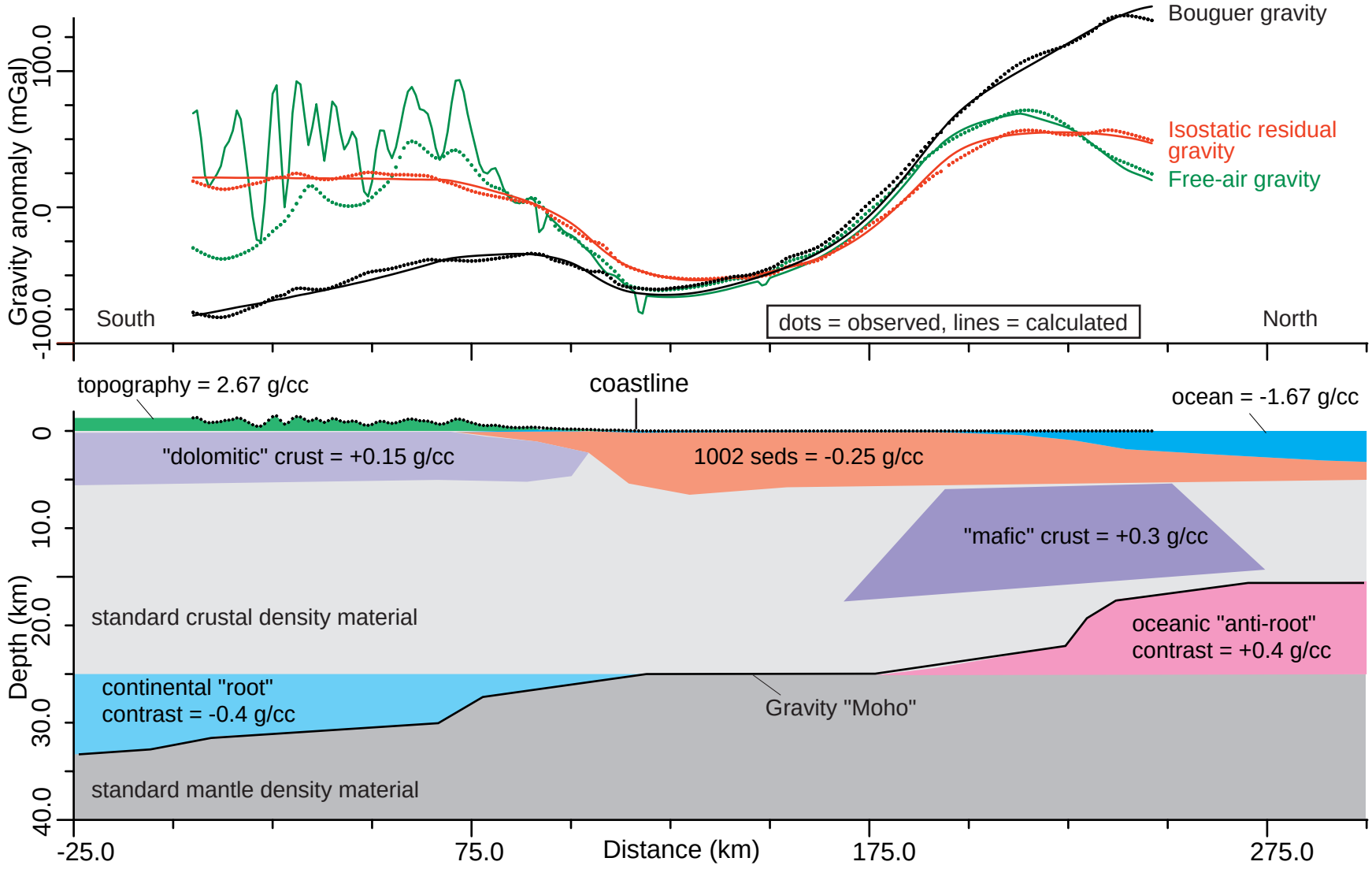

Figure GR2 - Saltus and others, 1998

Figure GR3. ANWR isostatic residual gravity

Isostatic residual gravity field with an illumination from the northwest. Gravity measurement locations are shown as dots.

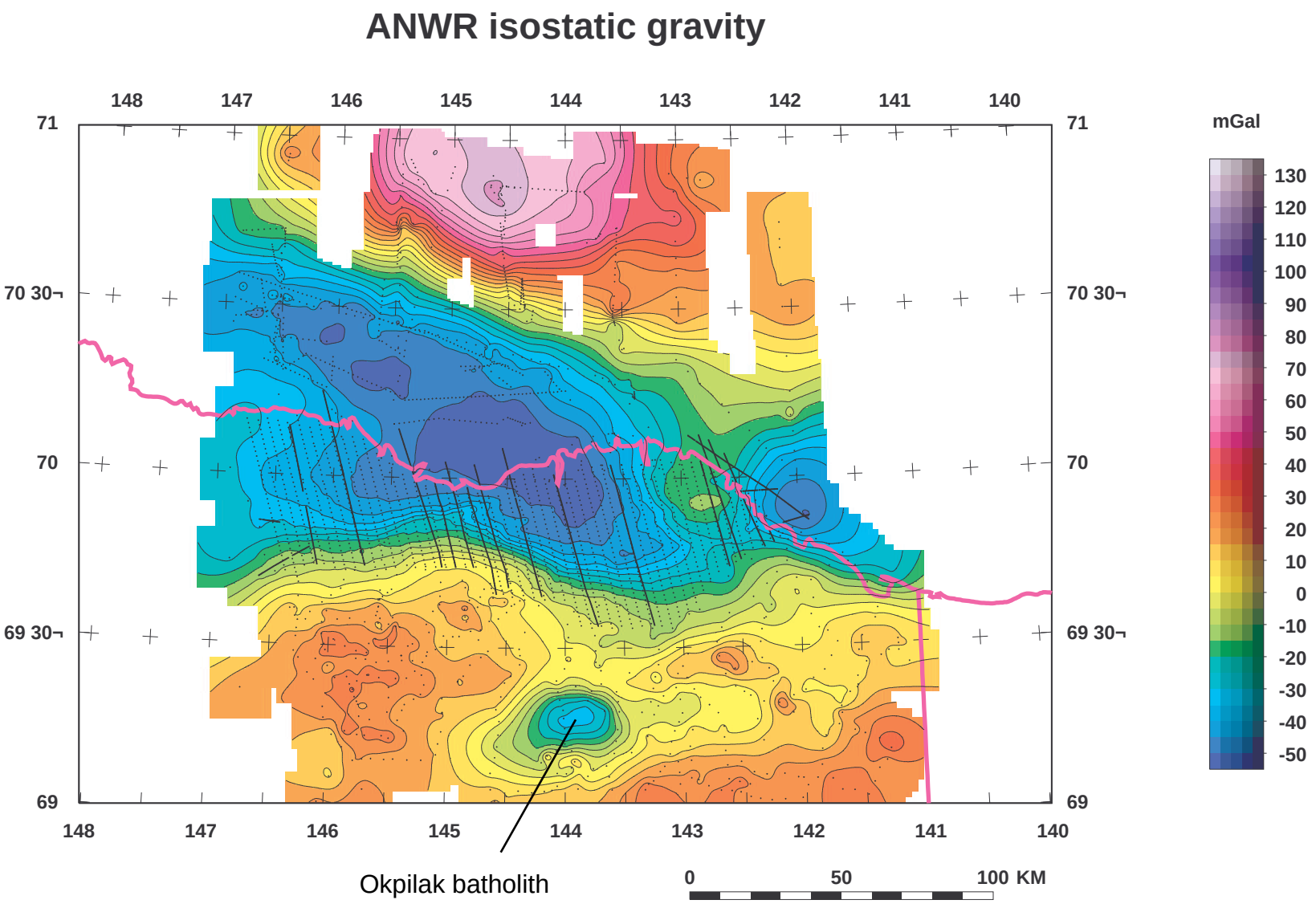

Figure GR4.
Rock density and stratigraphy
A summary of rock density information plotted on a stratigraphic column for northeastern Alaska. Surface density samples from Kososki and others (1978) are shown by a symbol combining a circle at the mean value and a horizontal line spanning the range of values for that rock type.
The number of samples and average (mean) values are listed next to the symbol. The vertical red lines are density determinations from borehole gravity (Beyer and Clutsom, 1989) in the Prudhoe Bay region to the west of the study area. The vertical black lines depict formation densities (based mostly on borehole density logs) used in modeling by Robbins (1987). The blue and purple lines are average densities inferred from scaled plots of borehole gamma-gamma density logs by Nelson (Chap. PP) and by us (blue lines). Dashed vertical lines indicate densities used in two-dimensional gravity modeling (see fig. GR5).

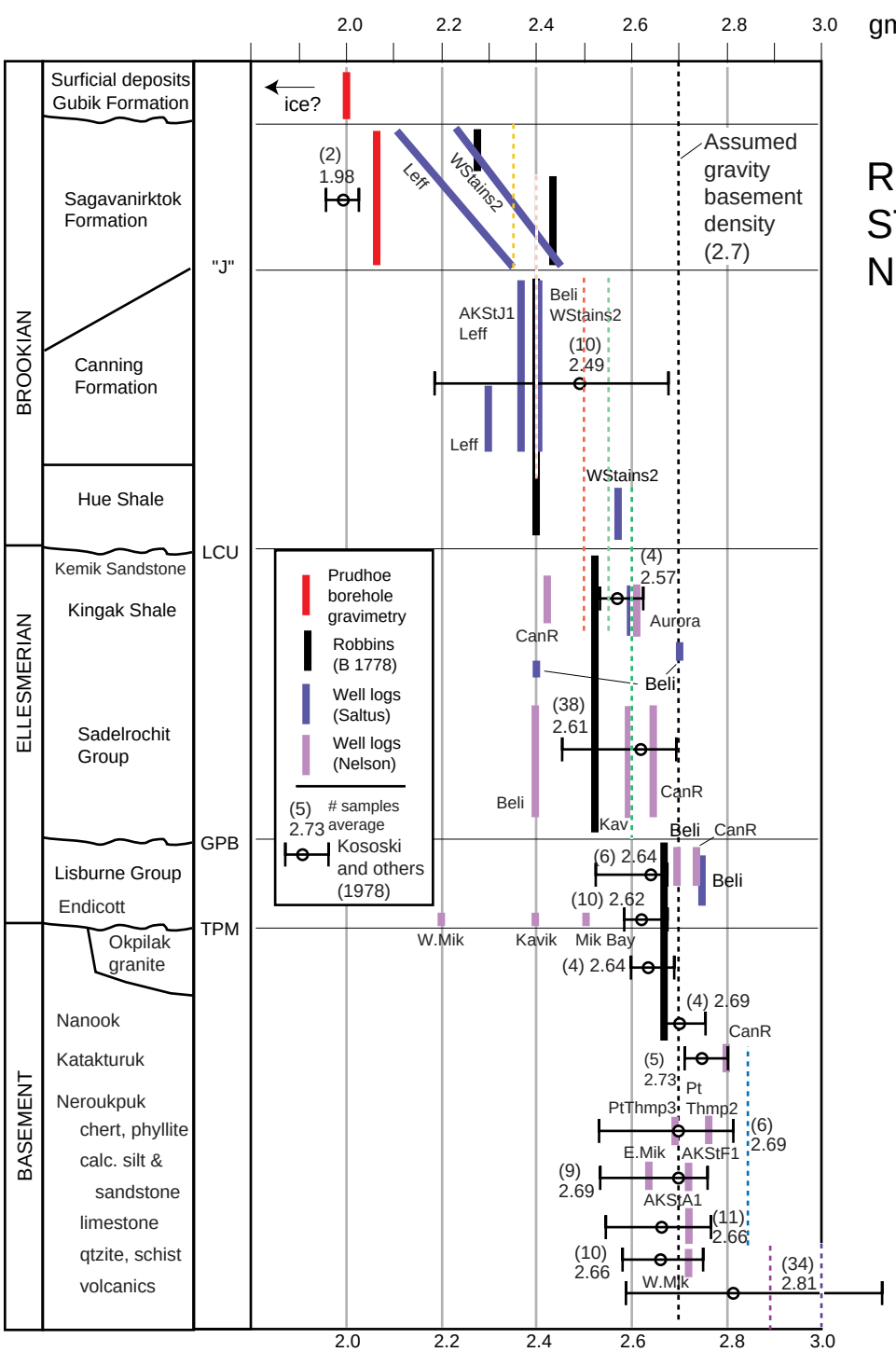

ROCK DENSITY & STRATIGRAPHY
NE Alaska

The Oil and Gas Resource Potential of the Arctic National Wildlife Refuge 1002 Area, Alaska
Open File Report 98-34

Figure GR5. Gravity model densities: color index

Eight density contrast units used in the gravity models of 6-11.

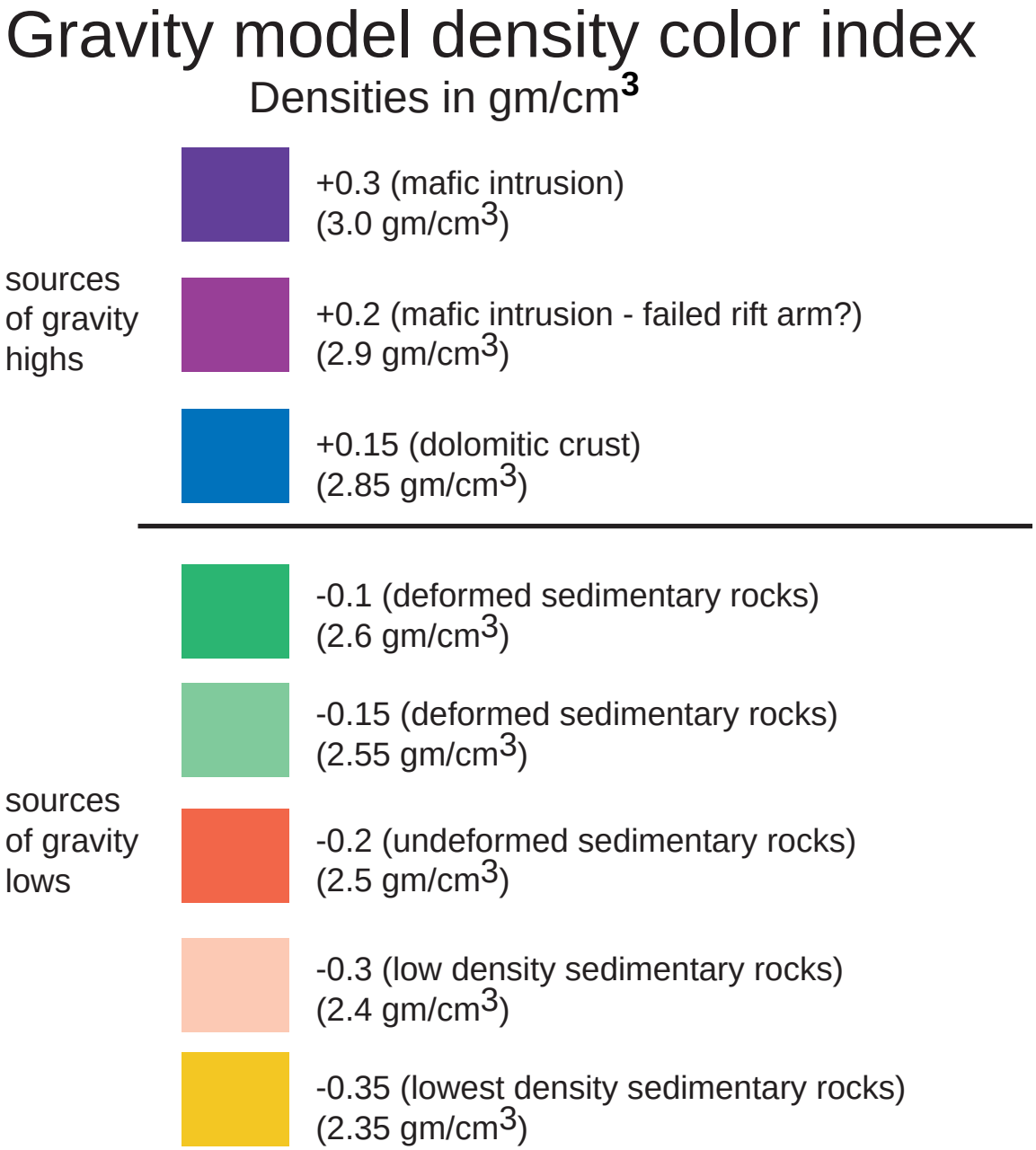

Figure GR6. 2D gravity model - seismic lines 84-6 & 85-8

Two-dimensional gravity model along seismic lines 84-6 and 85-5 (see fig. GR1 for location). The density units are defined in figure GR5. Primary reflective horizons as defined by the migrated seismic data are shown as black lines. The intersection of seismic line 84-3 is shown.

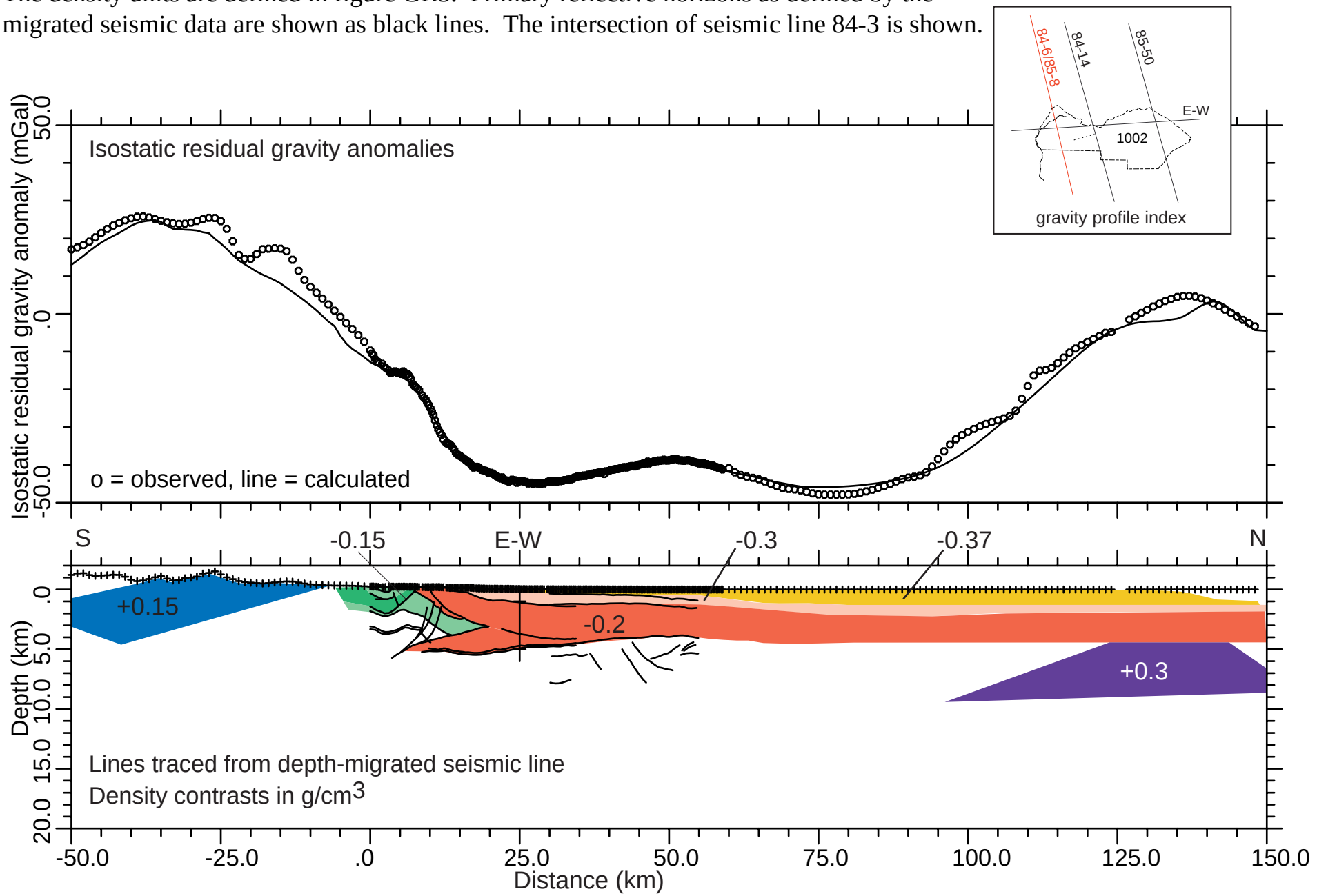

Figure GR7. Alternate 2D gravity model - seismic lines 84-6 & 85-8

Alternate model for the profile through seismic lines 84-6 and 85-8. Black lines are from a balanced cross section constructed by Cole (1998). Most of the density units are defined in figure GR5. At the south end of the profile the north-directed thrust sheets are modeled with a density contrast of +0.1 g/cm3 (corresponds to an absolute density of 2.8 g/cm3) with a surficial unit with a contrast of -0.05 g/cm3 (corresponds to an absolute density of 2.65 g/cm3).

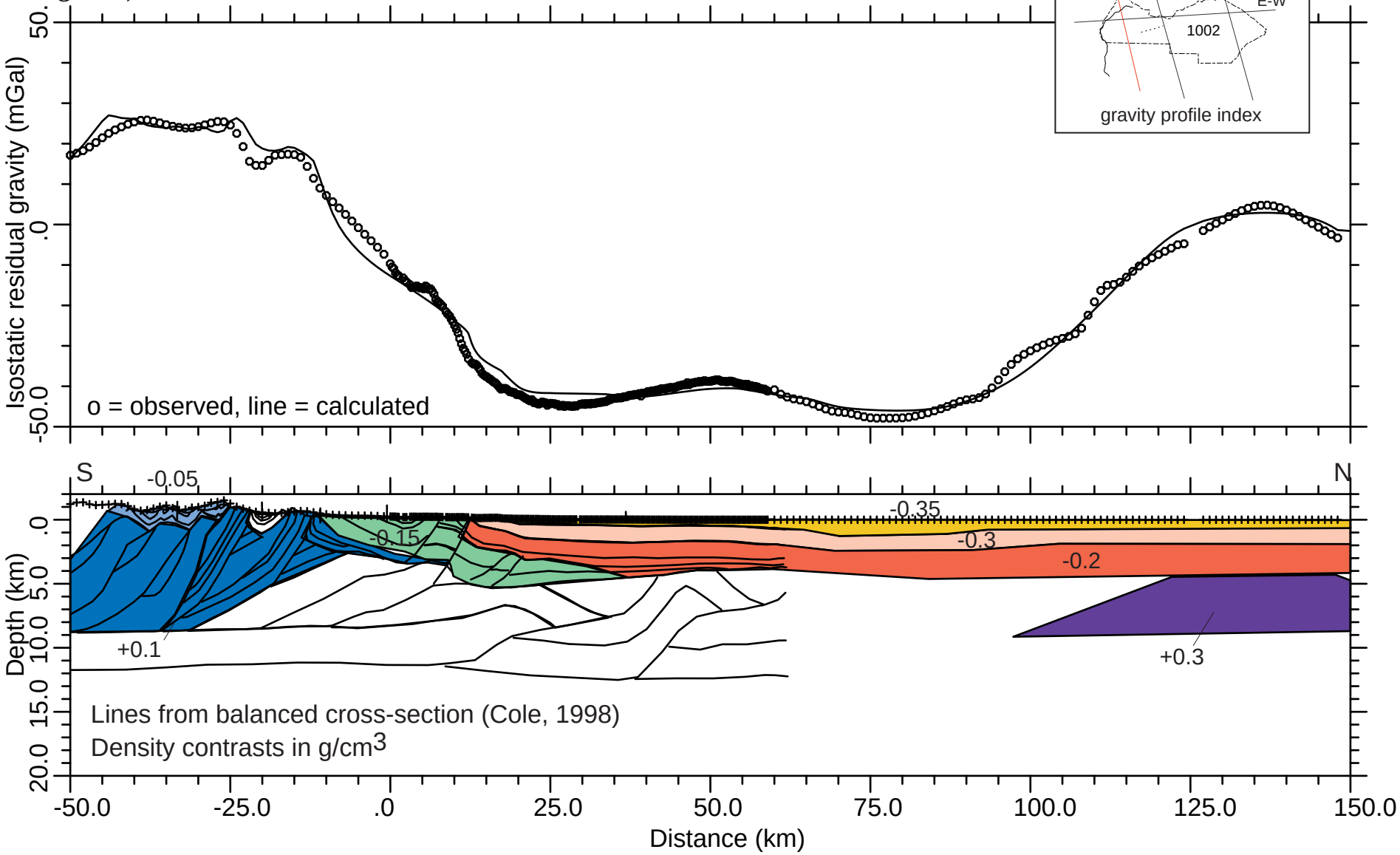

Figure GR8. 2D gravity model - seismic line 84-14

Two-dimensional gravity model along seismic lines 84-14 (see fig. GR1 for location). The density units are defined in figure GR5. Primary reflective horizons as defined by the migrated seismic data are shown as black lines. The intersection of gravity profile E-W is shown. MCA = Marsh Creek anticline.

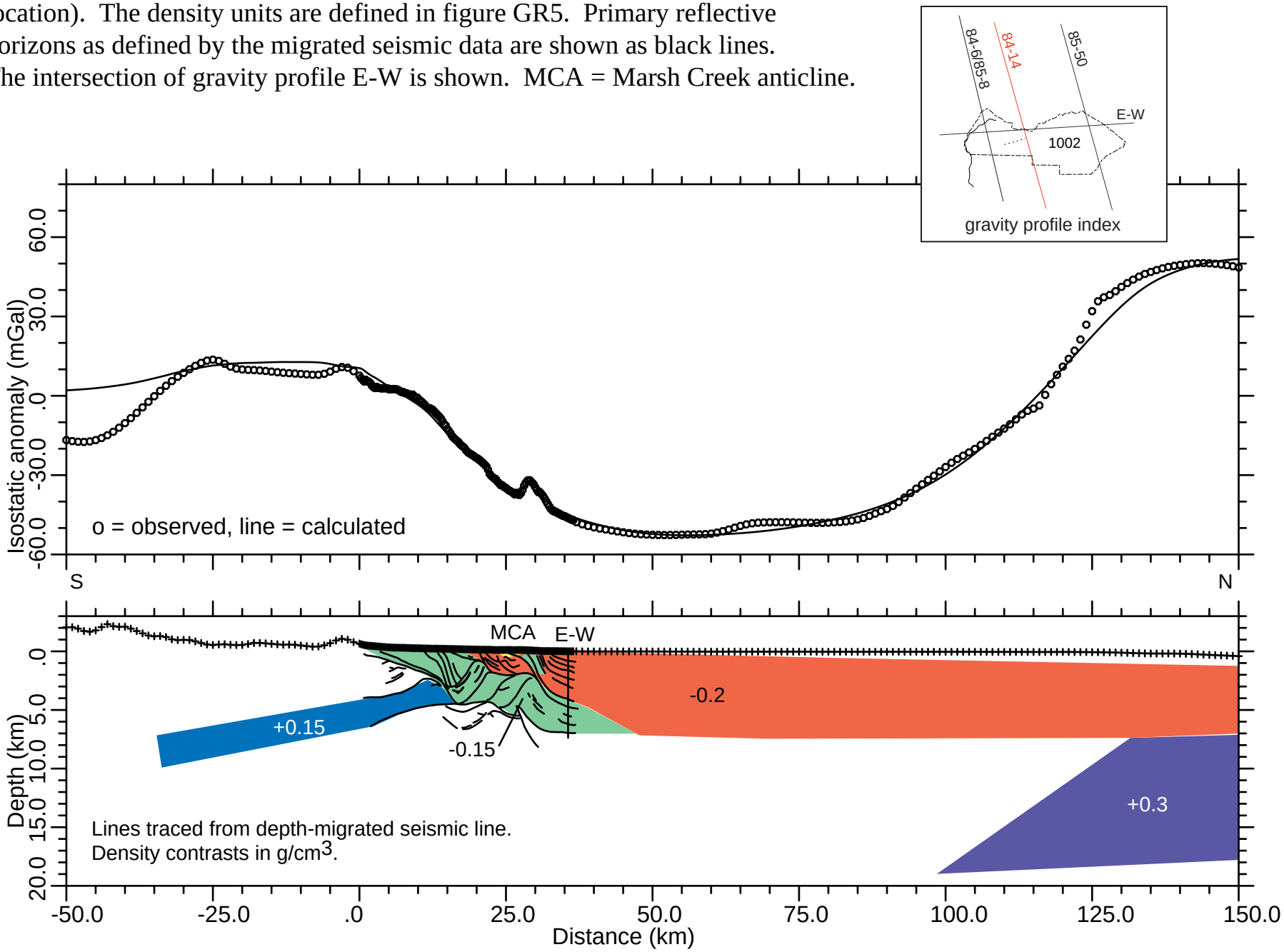

Figure GR9. 2D gravity model - seismic line 85-50

Two-dimensional gravity model along seismic lines 85-50 (see fig. GR1 for location).
The density units are defined in figure GR5. Primary reflective horizons as defined by
the migrated seismic data are shown as black lines. The intersection of gravity profile E-W is shown.

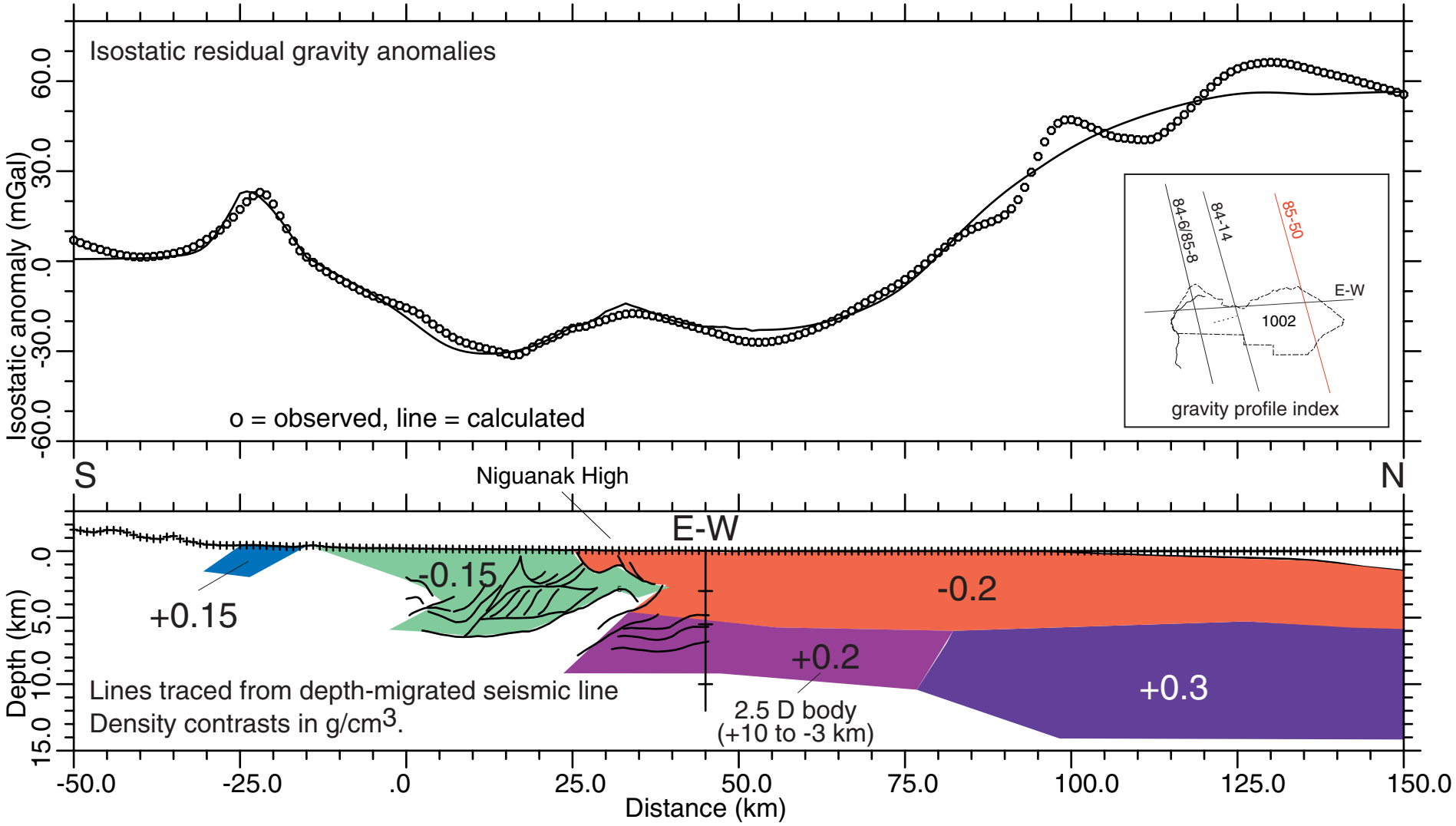

Figure GR10. 2D gravity model - E-W

Two-dimensional gravity model along an east-west gravity profile (see fig. GR1 for location).
The density units are defined in figure GR5. TPM horizon from Grow (1998) shown as black line.
The intersections of seismic lines 84-6, 84-14, and 85-50 are shown.

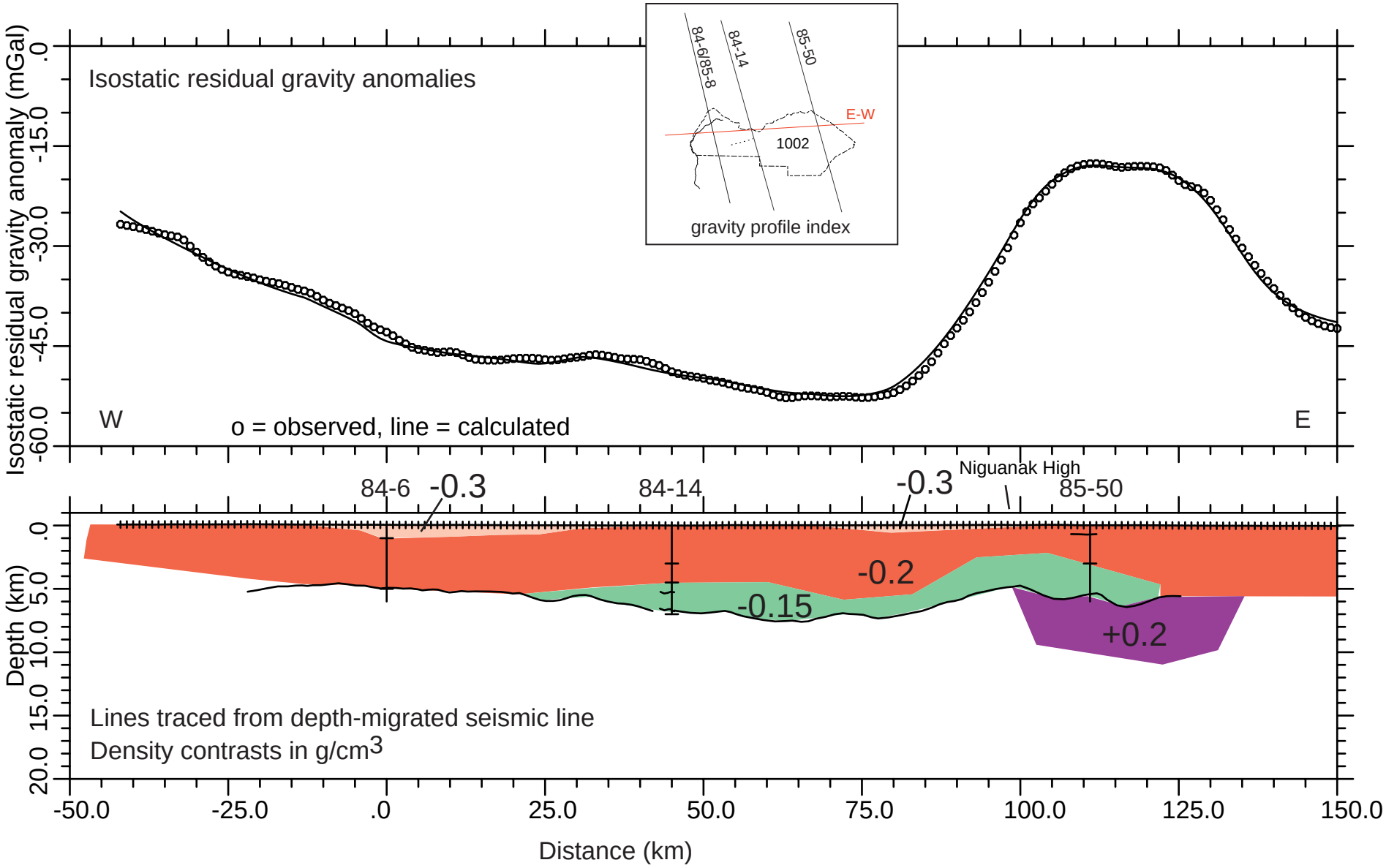

Figure GR11. 3D combined view of 2D gravity models

Three-dimensional perspective view of the two-dimensional gravity models along seismic lines 84-6/85-5, 84-14, 85-50, and gravity profile E-W (see fig. GR1 for locations). The density units are defined in figure GR5. Primary reflective horizons as defined by the migrated seismic data are shown as black lines.

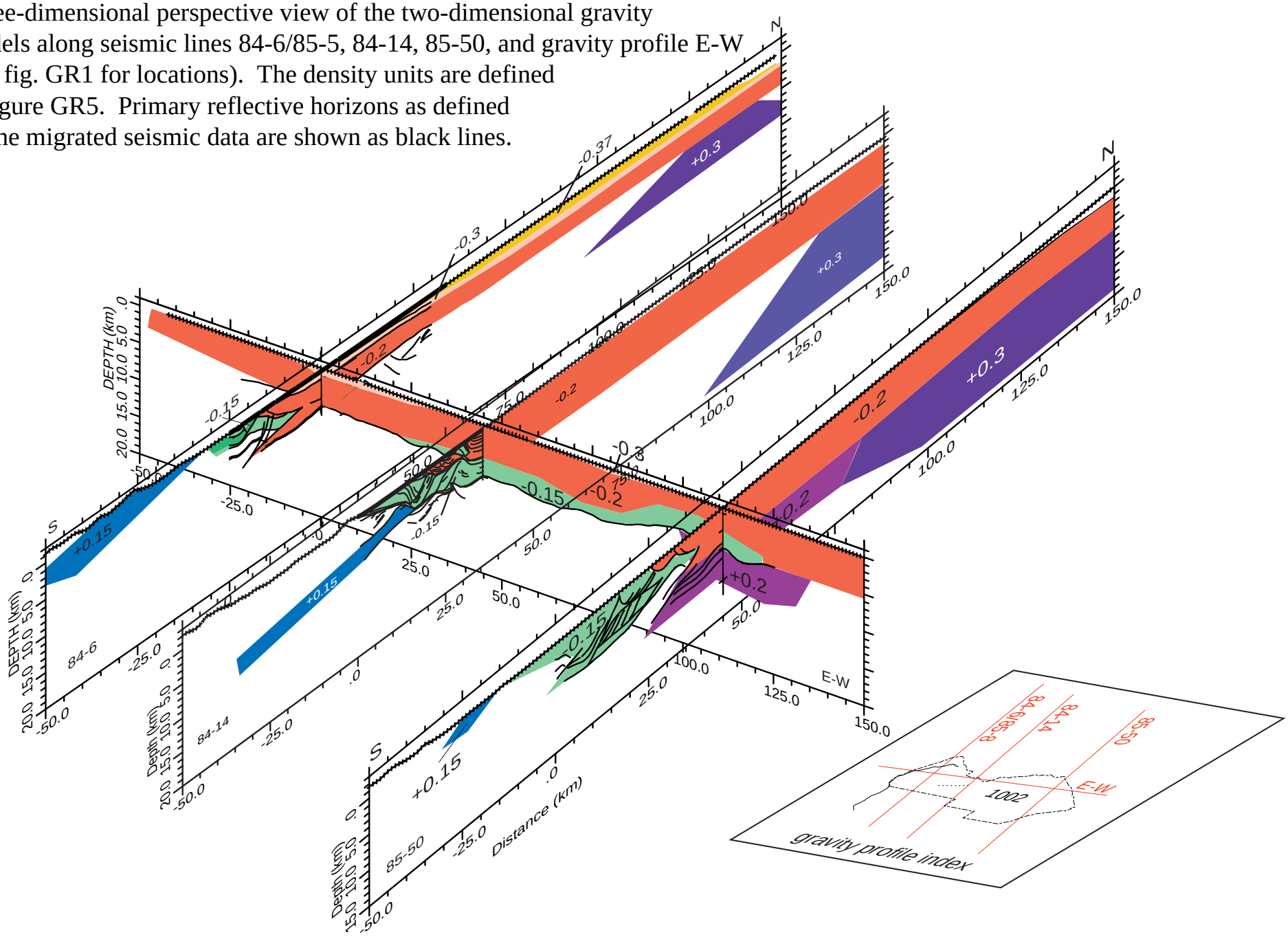

Figure GR12. Frequency separation - matched filtering of gravity data
Wavenumber (or spatial frequency) spectrum of the isostatic residual gravity field shown in figure GR3. The inset figure shows the separation of this spectrum into long, intermediate, and short wavelength bands based on matched filtering.

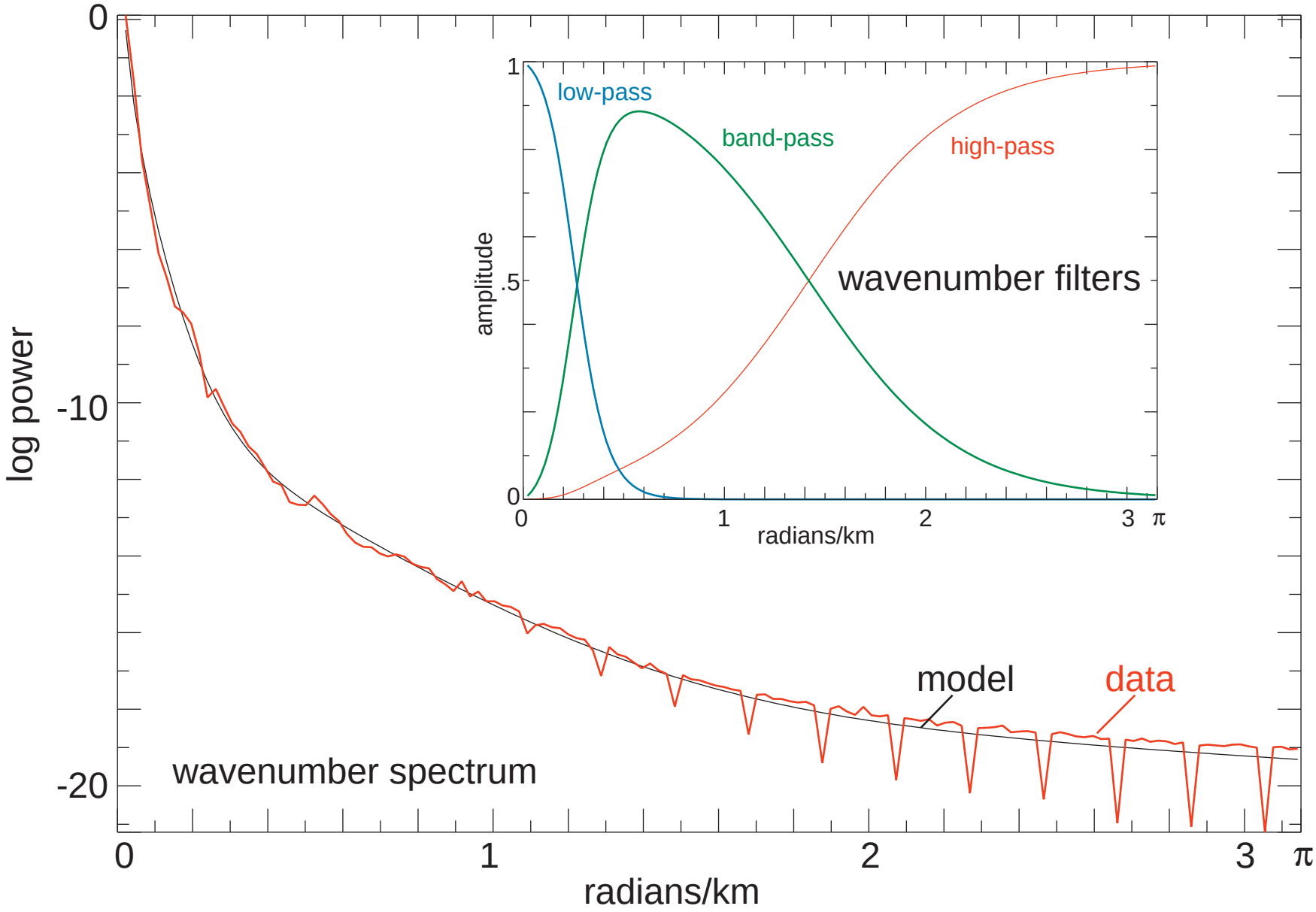

Figure GR13. Low-pass isostatic gravity map

This map shows the long wavelength portion of the isostatic residual gravity field that results from the application of the low-pass filter shown in Fig. GR12. These anomalies are primarily caused by variations in the depth to pre-Mississippian basement and by density contrasts within the pre-Mississippian basement.

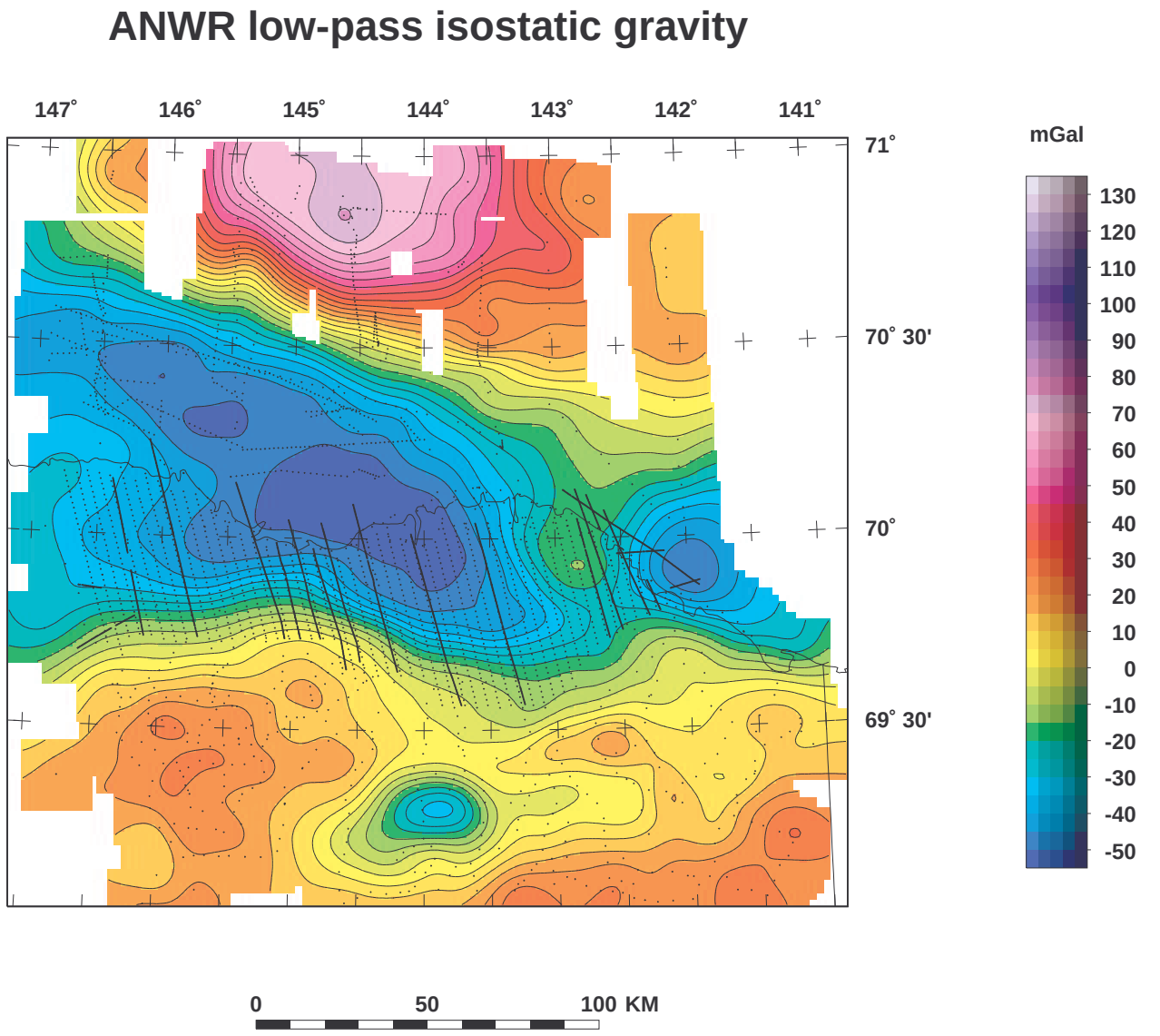

Figure GR14. high-pass gravity map

Intermediate and short wavelength portion of the isostatic residual gravity field that results from application of the band-pass and high-pass filters shown in Fig. GR12. These anomalies are primarily caused by structures within the Brookian section (in the upper 3 km).

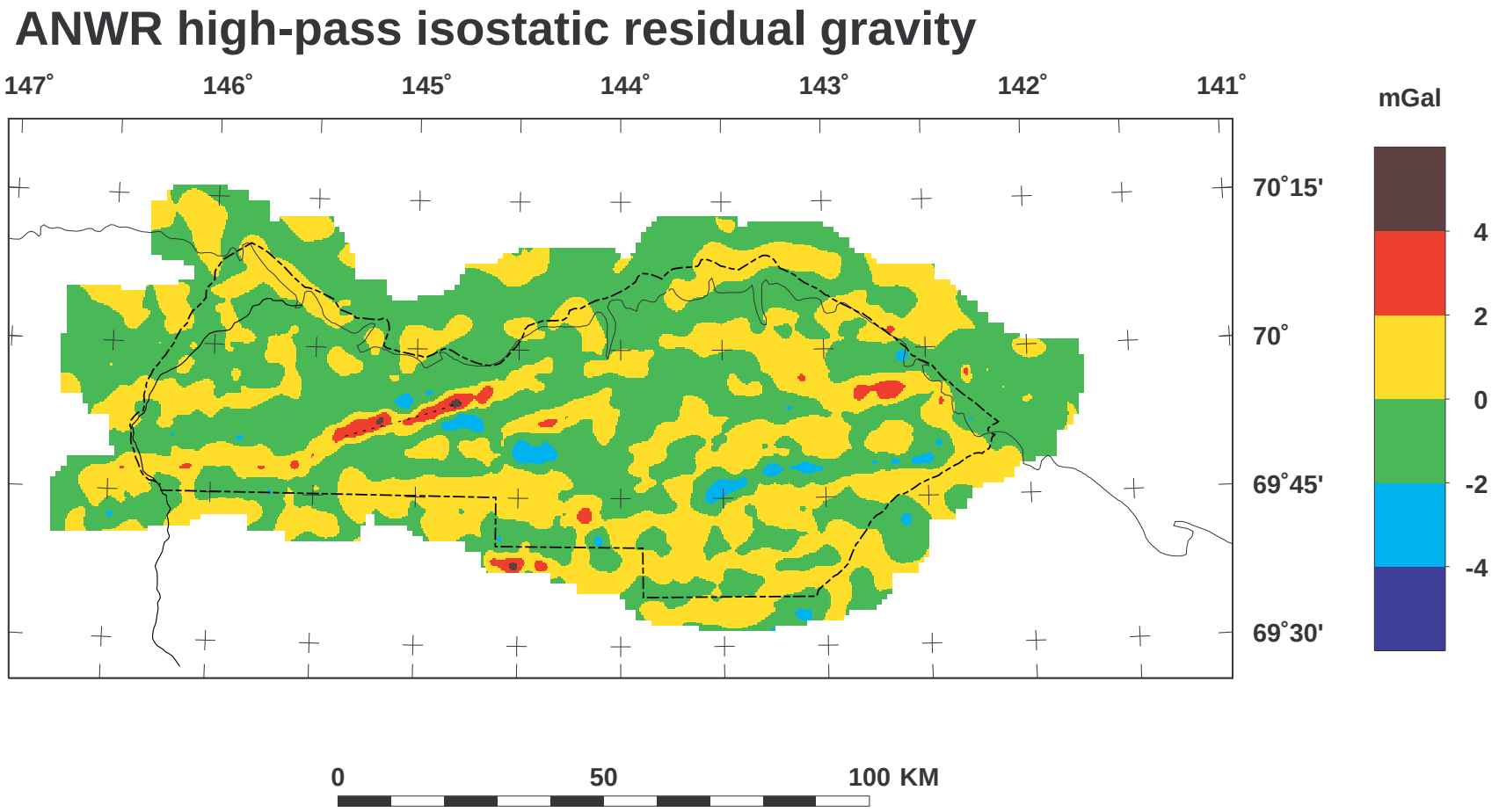

Figure GR15. 2D high-pass gravity model - seismic lines 84-6 & 85-8

Two-dimensional gravity model of the intermediate and short wavelength portion of the isostatic residual gravity field along seismic line 84-6. Seismic reflectors (heavy lines) and bodies modeled from aeromagnetic data (lighter lines; Phillips, 1998) are shown for reference. The gravity bodies are somewhat ad hoc, they are meant to give a feeling for the range of volumes and density contrasts required to fit these gravity features.

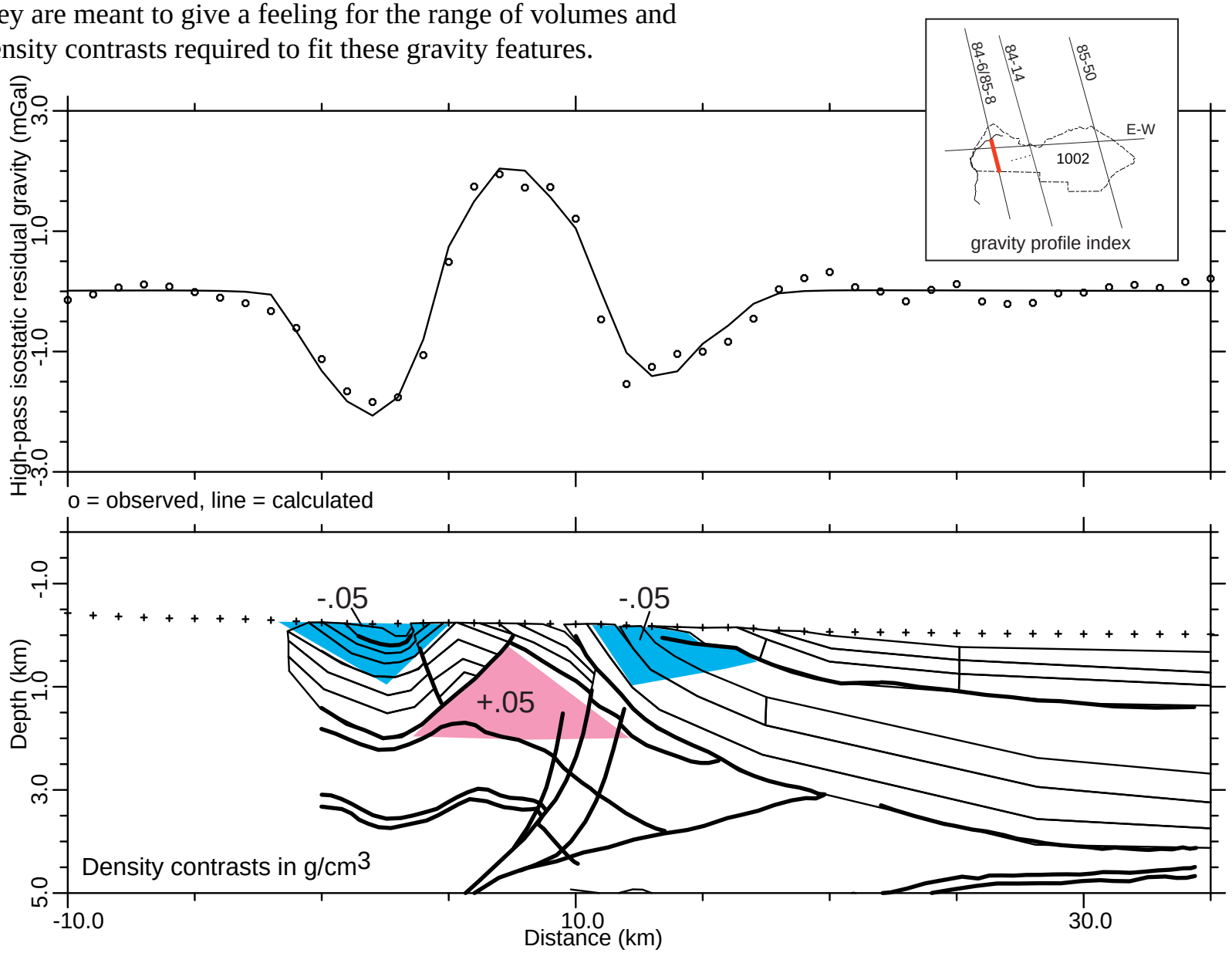

Figure GR16. 2D high-pass gravity model - seismic line 84-14

Two-dimensional gravity model of the intermediate and short wavelength portion of the isostatic residual gravity field along seismic line 84-14. Seismic reflectors (heavy lines) and bodies modeled from aeromagnetic data (lighter lines; Phillips, 1998) are shown for reference. The gravity bodies are somewhat ad hoc, they are meant to give a feeling for the range of volumes and density contrasts required to fit these gravity features.

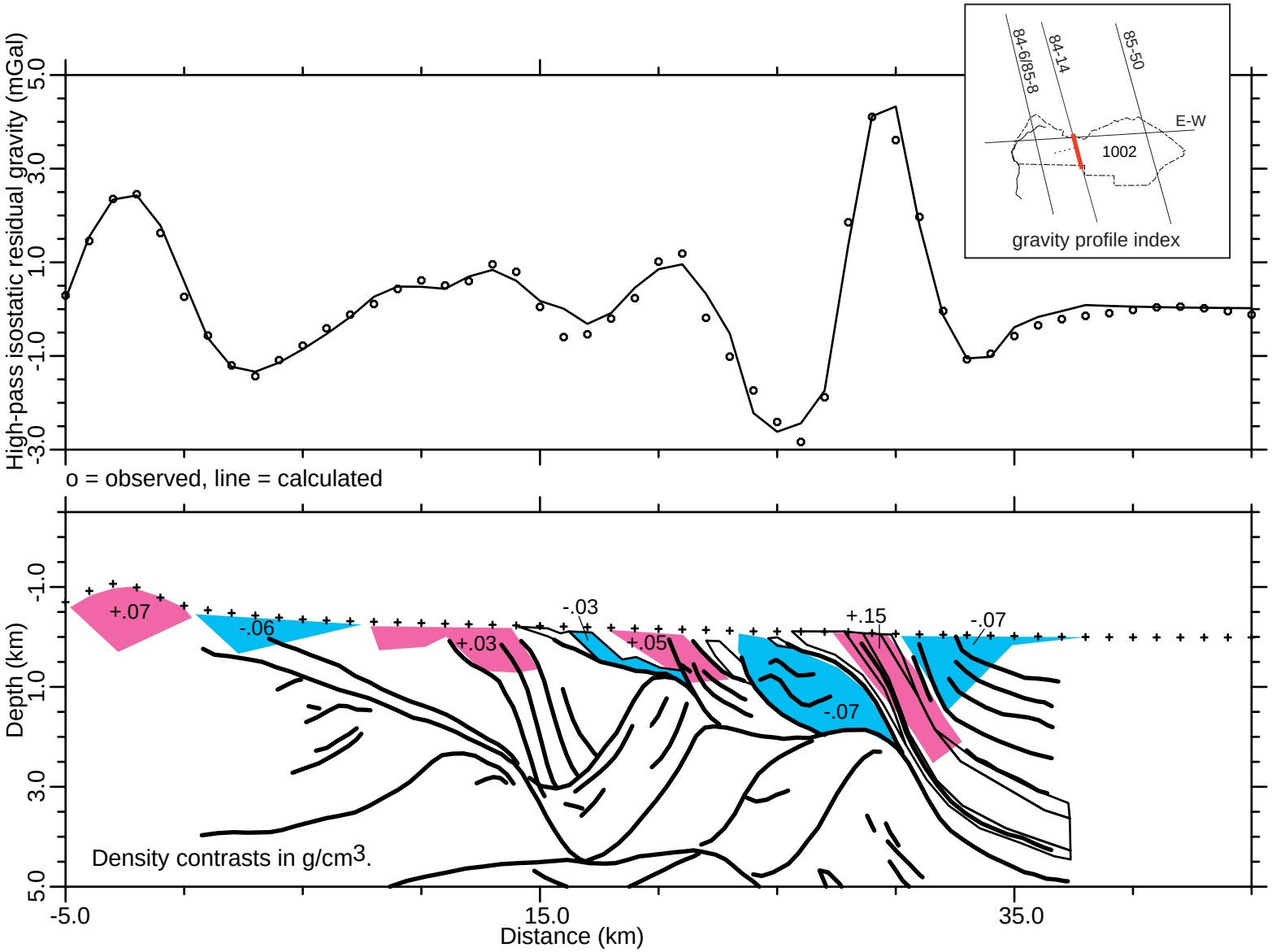

Figure GR17. 2D high-pass gravity model - seismic line 85-50.

Two-dimensional gravity model of the intermediate and short wavelength portion of the isostatic residual gravity field along seismic line 85-50. Seismic reflectors (heavy lines) and bodies modeled from aeromagnetic data (lighter lines; hotkey to Phillips, 1998) are shown for reference. The gravity bodies are somewhat ad hoc, they are meant to give a feeling for the range of volumes and density contrast required to fit these gravity features.

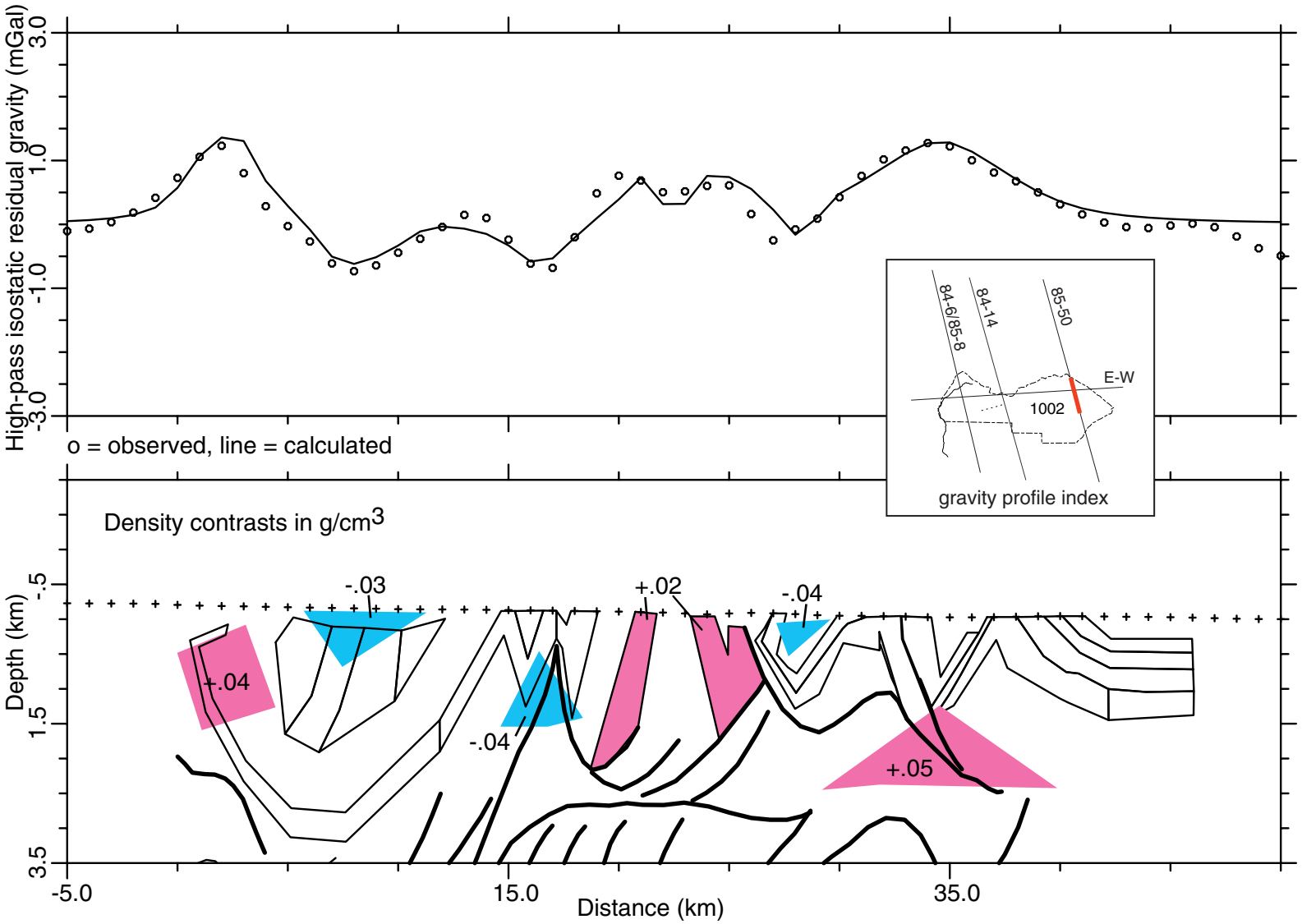

Figure GR18. 3D structure map from high-pass gravity

Map of the density interface that results from fitting the intermediate and short wavelength residual gravity field (fig. GR14) with a single layer model with a density contrast of 0.1 g/cm^3. The model shows a number of ridges that correlate with seismically defined structures (including the Marsh Creek anticline, fig. GR1).

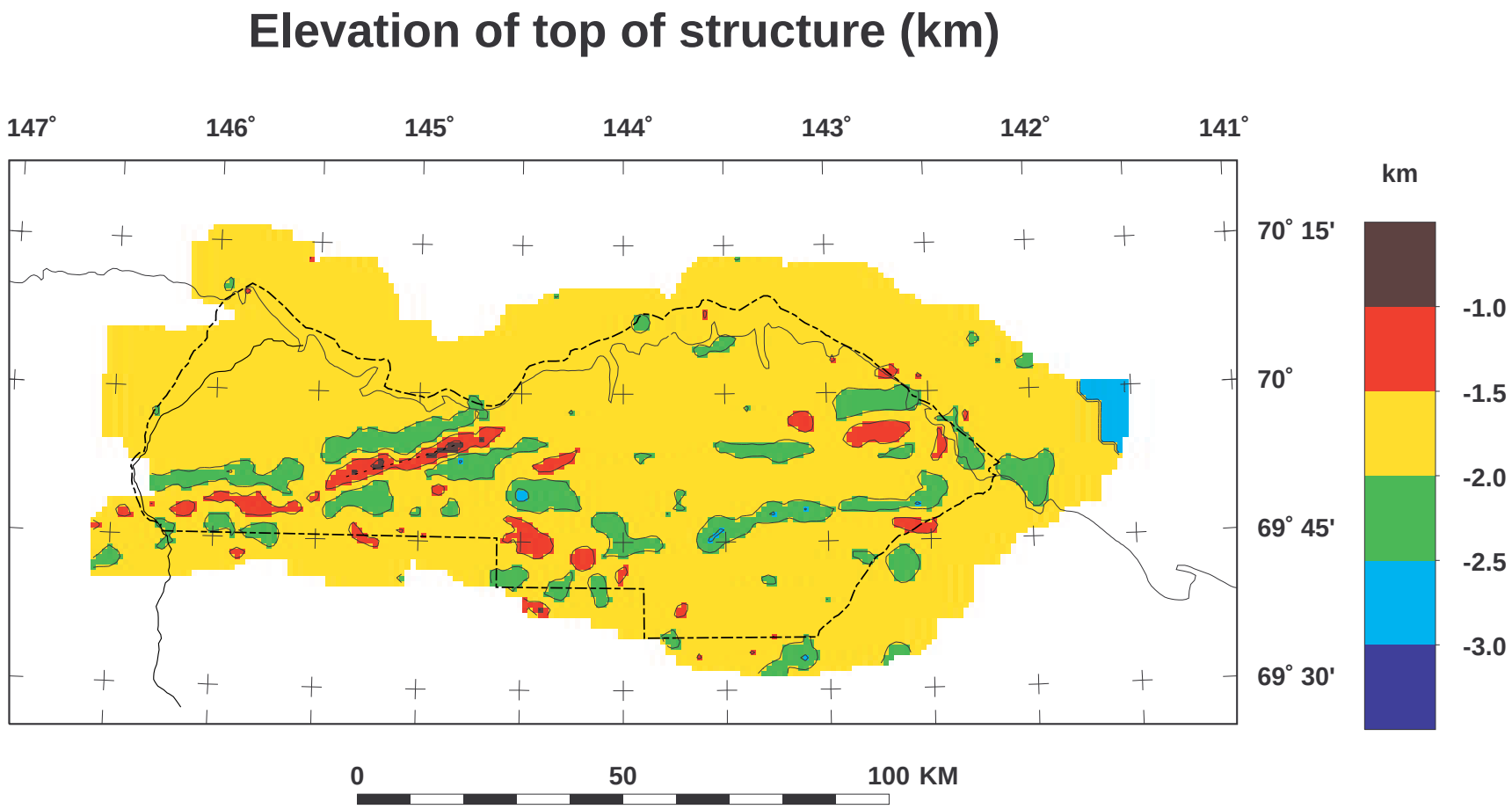

Figure GR19. 3D structure map with selected structures identified
This map shows the location of 12 structures for which we have calculated areas and volumes (table GR1).

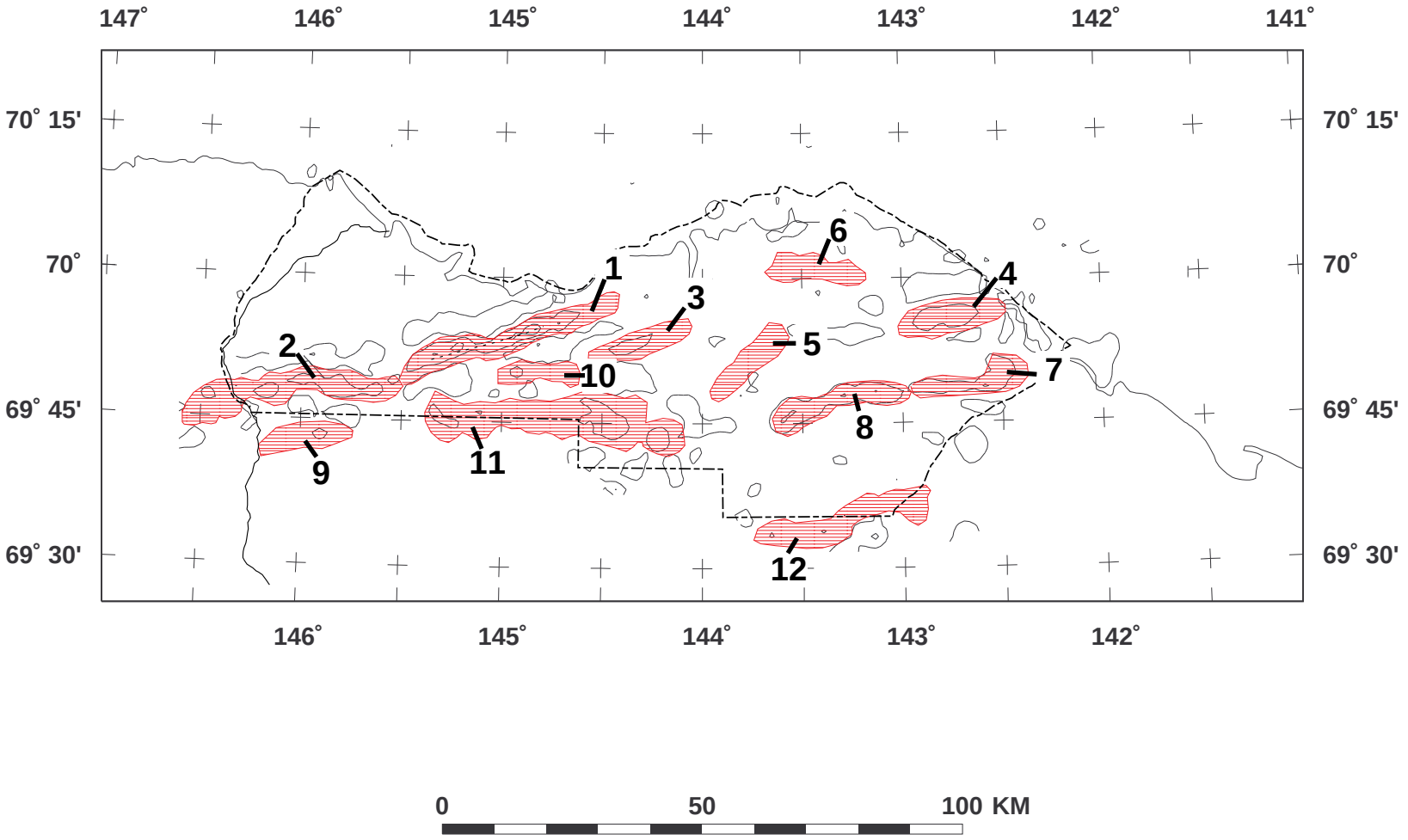

Plate GR1 - ANWR isostatic residual gravity map
Isostatic residual gravity field with an illumination from the northwest. Gravity measurement locations are shown as dots. This plate is the same map as Fig. GR3, but at larger scale.

ANWR isostatic residual gravity

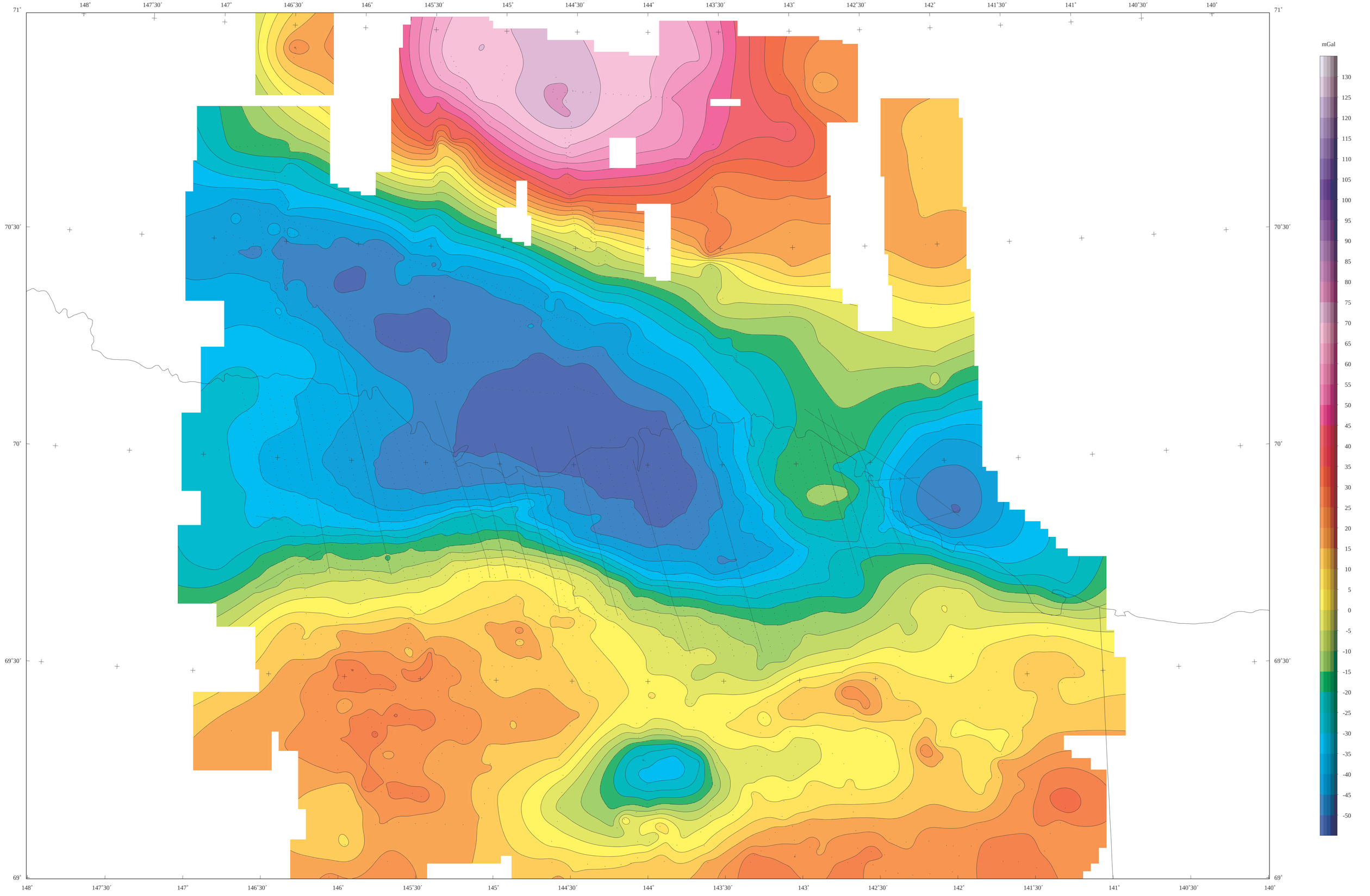

0 50 100 KM

USGS science for a changing world

The Oil and Gas Resource Potential of the Arctic National Wildlife Refuge 1002 Area, Alaska
Open File Report 98-34